Chiara Modanese

Impact of compensation on solar grade silicon for photovoltaics

Thesis for the degree of Philosophiae Doctor

Trondheim, February 2012

Norwegian University of Science and Technology
Faculty of Natural Sciences and Technology
Department of Materials Science and Engineering

NTNU – Trondheim
Norwegian University of
Science and Technology

NTNU
Norwegian University of Science and Technology

Thesis for the degree of Philosophiae Doctor

Faculty of Natural Sciences and Technology
Department of Materials Science and Engineering

ISBN 978-82-471-3369-9 (printed ver.)
ISBN 978-82-471-3370-5 (electronic ver.)
ISSN 1503-8181

Doctoral theses at NTNU, 2012:51

Printed by NTNU-trykk

Procrastination gives you something to look forward to.

- Joan Konner

Preface

The work presented in this thesis has been carried out primarily at the Norwegian University of Science and Technology (NTNU) at the Department of Materials Science and Engineering. The thesis was completed during the period from November 2007 to December 2011 as a part of the Norwegian research project *Control of impurities in metallurgically refined silicon for solar cells*. The partners in the project have been NTNU, SINTEF, Elkem Solar AS, CruSiN AS / Saint Gobain.

Two periods in the Autumn 2010 and Spring 2011 (two months and one week, respectively) were spent at the Department of Materials Science at the University of Milano Bicocca (Italy).

The thesis consists of two parts. The first part is an introduction to compensation in solar grade crystalline silicon materials for photovoltaic applications. The focus is on the impact of dopant compensation and on the interaction between dopant species and other main impurities. A description of the materials studied and of the main characterization techniques employed is provided in a separate chapter.

The second part consists of published/submitted articles which present the results of the experimental work that has been carried out. The following manuscripts are included:

Article 1:
Chiara Modanese, Marisa Di Sabatino, Anne-Karin Søiland, Kristian Peter, Lars Arnberg, *Investigation of bulk and solar cell properties of ingots cast from compensated solar grade silicon*, Progress in Photovoltaics: Research and Applications 19 (2011) 45-53

Article 2:
Chiara Modanese, Marisa Di Sabatino, Anne-Karin Søiland, Lars Arnberg, *Relationship between net doping density and resistivity of compensated mc-Si ingots*, Physica Status Solidi C 8 (2011) 713-716

Article 3:
Chiara Modanese, Maurizio Acciarri, Simona Binetti, Anne-Karin Søiland, Marisa Di Sabatino, Lars Arnberg, *Temperature-dependent Hall-effect measurements of p-type multicrystalline compensated solar grade silicon*, submitted to/under review in Progress in Photovoltaics: Research and Applications, November/December 2011

Article 4:
Chiara Modanese, Marisa Di Sabatino, Martin Syvertsen, Lars Arnberg, *Bulk properties of multicrystalline silicon ingots for solar cells cast in silicon nitride crucibles*, to be submitted to Journal of Crystal Growth, February 2012

Article 5:
Madeleine Hystad, Chiara Modanese, Marisa Di Sabatino, Lars Arnberg, *Distribution and impact of chromium in compensated solar grade silicon*, submitted to/under review in Solar Energy Materials and Solar Cells, May/November 2011

Trondheim, December 2011

Chiara Modanese

Acknowledgements

First of all, I would like to express my deepest gratitude to my main supervisor, Professor Lars Arnberg. He has been a precious guide during my work and his door has always been open, whether for scientific discussion, professional advice or personal one. I appreciated his encouraging words in many an occasion.

Marisa Di Sabatino Lundberg deserves a giant thank-you. She has been a very thoughtful and dedicated co-supervisor, always present for an advice on scientific matter or general issues. I feel privileged in having had the possibility to learn so much from her. Moreover, I am extremely grateful for the time she took for proof-reading during her maternity leave.

I would like to thank the partners in the BIP-Light Elements project (Contract nr. 180107/I40) and the Norwegian Research Council for funding. In particular, my thanks go to the project leader Ragnar Fagerberg (SINTEF); Anne-Karin Søiland (Elkem Solar AS), especially for having been a very patient and dedicated mediator; Martin Syvertsen, Helen Langeng and Birgit Ryningen (SINTEF), Martin Bellmann (NTNU/SINTEF), Håvard Sørheim and Arve Solheim (Crusin AS/Saint Gobain) for their precious collaboration.

I had the opportunity to work with the group of Ass. Prof. Simona Binetti and Dr. Maurizio Acciarri at University of Milano Bicocca. I am grateful to them for welcoming me in their group and for making my stay in Milan a successful one. Fellow PhD student Andrea Scaccabarozzi has been very helpful in his assistance with the Hall-effect measurements.

I have had the great possibility to work with several students during my work. The collaboration with Madeleine Hystad, Janine Friedl, Aleksander Rise Gallala and Martino Danuso has been very interesting, both on the scientific and on the personal side.

There are many people at NTNU and SINTEF that have kindly helped me during my work. Among them, I would like to thank in particular Torild Krogstad (etching and GDMS), Birgitte Karlsen (polishing and etching), Yu Hu (etching), Yingda Yu (SEM), Gaute Stokkan (discussions), Ove Darell (ingot cutting), Hilde Martinsen Nordø, Unni Keiseraas, Brit Wenche Meland, Hege Knutsdatter Johnsen, Elin Kaasen and Åse Lill Salomonsen (administrative work).

My memory goes to the late Anne Lise Dons, who had been very kind when I started at NTNU and had taught me a great deal on the GDMS, including how to be patient with it.

Rune Søndenå, Arve Holt and Bent Thomassen at IFE are gratefully acknowledged for their timely assistance with lifetime measurements. Moreover, I express my gratitude to Rune Søndenå for his patient and precise contribution with laser cutting.

My years in Trondheim have been so wonderful thanks to the contribution of friends, within and outside the university. Thank you!

Infine voglio ringraziare la mia famiglia, che mi ha permesso di arrivare dove sono e che ha sempre appoggiato le mie decisioni, seppure qualche volta a malincuore. Grazie di cuore ☺

Moreover, there are few other aspects which I would also like to acknowledge. These last years would have been much less enjoyable if it were not for …

… the English language, which taught me peculiar expressions such as indeed, happily situated, rather distressed, proper, brilliant.

… the five rejected applications for the Norwegian course in Dragvoll, which considerably speeded up my learning.

… friends in Trondheim, who usually did not escape the GDMS updates, and more generally supported me in always giving 100% at work.

… the GDMS, which has always run so smooth and nice.

… Janine, who taught me how to throw the chocolate eyes.

… Katharina, whose forwarded links greatly helped me with procrastinating tasks.

… Marina, who showed her strong support on publication-related issues.

… Marisa, who told me that, generally speaking, Valencia tends to be in Spain, not in Germany.

… Martin S., who credited me with the distinguished honour and responsibility of switching on the gas measurements in the middle of the night.

… my exchange period abroad, which actually happened to be in Italy.

… my office mates, who have been either rather silent or rather talkative.

… my parents, who gave up suggesting me job opportunities in Italy after two mere, short years in Norway.

Abstract

The steep increase in the market price for silicon feedstock for solar cells experienced at the beginning of the last decade, coupled with a developing industry, opened the possibility for materials produced from different sources and delivered at lower production cost. Compensated solar grade silicon for solar cell provided these opportunities. The motivation behind the present work was, therefore, to study the effect of such a material on the bulk and cell properties, in respect to the commonly used feedstock produced via the Siemens process. The materials presented in this work were produced at Elkem Solar AS, who has provided materials with decreasing dopant concentration over the project time.

The main focus was to investigate the manner in which materials cast from compensated solar grade feedstock behave compared to materials cast from reference electronic grade feedstock. Different properties were measured, both in the bulk and on solar cells. Resistivity was observed to increase along the growth direction due to the different segregation profiles of the main doping species, *i.e.* boron and phosphorus. Dissolved oxygen concentration was observed not to depend on feedstock, whereas higher dissolved carbon concentration was measured in the compensated materials. Minority carrier lifetime is reduced, although the performance of the materials after solar cell processing is comparable to the electronic grade reference materials. Majority carrier mobility is strongly reduced at temperatures below 150 K, whereas the reduction at high temperatures (above 250 K) is much lower.

The possibility to use international standards to convert the measured resistivity in net doping density for compensated materials was investigated. The aim was to provide an easy and direct method to assess these materials. Through the comparison of the net doping density calculated from the measured resistivity and the net doping density measured by glow discharge mass spectrometry, the accuracy of the standard was evaluated for the compensated materials.

Silicon nitride crucibles are an alternative to the widely used silica crucibles for directional solidification of mc-Si ingots. Their main advantages are reusability for repeated castings and the opportunity to eliminate the crucible as a source of oxygen contamination of the ingot. In this work, several ingots cast in such crucibles were studied and compared to ingots cast in silica crucibles. Advantages and limitations related to the use of such crucibles are discussed, with focus on the required changes to the solidification process.

Chromium is an impurity known to be detrimental for the material quality of silicon for solar cells. Its effect is of particular interest for less pure materials such as those studied in this work, where the concentration of Cr can be expected to be greater than in electronic grade materials. The impact of Cr on the properties of the compensated solar grade silicon materials was studied through the comparison of ingots with and without deliberate chromium doping. It was found that, although minority carrier lifetime is significantly impaired by the addition,

a strong improvement occurred through adequate solar cell processing, which included a phosphorus diffusion step.

List of symbols and abbreviations

A	absorbance
B_s	substitutional boron
c-Si	crystalline silicon
C_l	compensation level
C_l	impurity concentration in the liquid
C_0	initial impurity concentration (in the melt)
C_s	impurity concentration in the solid
C_s	substitutional carbon
CZ-Si	Czochralski silicon
ΔV_H	Hall voltage
D_n, D_p	electron, hole diffusion coefficient
E	electric field
E_C	conduction band energy
EG-Si	electronic grade silicon
η	efficiency of solar cell
FF	fill factor of solar cell
FPP	four point probe
FTIR	Fourier transform infrared spectroscopy
FZ-Si	float-zone silicon
GDMS	glow discharge mass spectrometry
IBR	ion/beam ratio
k_0	equilibrium segregation coefficient
J_{SC}	short circuit current density of solar cell
LID	light induced degradation
L_n, L_p	electron, hole diffusion length
μ_C	conductivity mobility
μ_H	Hall mobility
μ_n, μ_p	electron, hole mobility
µw-PCD	microwave photoconductance decay
mc-Si	multicrystalline silicon
MG-Si	metallurgical grade silicon
N_A, N_D	acceptor, donor density
N_B, [B]	atom boron concentration
O_i	interstitial oxygen
p_0	hole density (net acceptor density)
poly-Si	polycrystalline silicon

ppba, ppbw	parts per billion atomic, weight
ppma, ppmw	parts per million atomic, weight
PV	photovoltaic
q	elementary charge
QSSPC	quasi-steady-state photoconductance decay
ρ	resistivity
R_C	compensation ratio
R_H	Hall coefficient
r_H	Hall factor
RSF	relative sensitivity factor
σ	conductivity
SoG-Si	solar grade silicon
T	transmittance
TD	thermal donors
τ_{eff}	effective minority carrier lifetime
τ_n, τ_p	electron, hole bulk lifetime
UMG-Si	upgraded metallurgical grade silicon
v_d	drift velocity of the charge carrier
V_{OC}	open circuit voltage of solar cell

Table of contents

Chapter 1

Introduction

The global electricity production in the year 2009 included approximately 19% from renewable energies [1], where nuclear power is excluded from the calculation. Among these renewable sources, hydroelectric energy is dominating, with a share of more than 84%, followed by wind energy at approximately 7%. Solar power has not reached significant proportions yet, as it is at 0.6% of the global electricity production in 2009, which corresponds to 21.4 TWh produced (20.5 TWh from photovoltaic and 0.9 TWh from solar thermal). Nevertheless, the solar energy production has experienced an average yearly growth rate of 36% in the decade 1999-2009, with its 2009 level similar to the 1999 level for wind energy, but with a much steeper increase. Moreover, the solar industry has now entered the mass production stage [1], which will allow for the steep progression trend to be sustained.

The photovoltaic market is strongly dominated by crystalline silicon technology, which accounts for about 86% of the global cell production in 2010 [2]. This value is dominated by multicrystalline (mc) over monocrystalline cells, which score approximately 53% and 33%, respectively. The mc-Si share corresponds to approximately 14.4 GW of installed power capacity during the year 2010 [2]. For the crystalline Si materials to uphold their current market position and face the emerging materials such as thin film silicon or CIGS (copper-indium-gallium-selenide), it is vital to decrease the production costs. According to the 2007 EU Strategic Research Agenda for Photovoltaic Solar Energy Technology [3], direct production costs of crystalline silicon solar cells are forecast to decrease to about 1 €/W_p by 2013, and this goal can be achieved through joint efforts on three main routes to cost saving, namely 1. reduction in materials consumption, 2. increase in device efficiency, and 3. advanced and high-throughput manufacturing. It is worth noting that the threshold of 1 €/W_p as factory-gate price has been already reached in summer 2011 [4]. With the aim at achieving these goals, the development and/or improvement of new, lower-cost and less energy-intensive processes to manufacture silicon feedstock could provide Si at production prices in the range 10-20 €/kg in the next years [3]. The threshold of ~18-20 €/kg is considered the limit to remain competitive in year 2012 in the case of upgraded metallurgical grade (UMG) silicon manufacturers [5].

During the last years, various low-cost, less energy-intensive processes for the refining of metallurgical grade (MG) silicon have been developed. Compared to the standard process used in the past decades by the PV industry and adapted from the electronics industry, *i.e.* the Siemens process, these new metallurgical refining routes have the clear advantage of a much lower energy consumption. For example, the power consumption rate at the Elkem Solar production plant in Norway is ~40 kWh/kg solar grade silicon (SoG-Si) produced, whereas the consumption rate is above 170 kWh/kg SoG-Si produced for a traditional Siemens process

[6]. Examples of these alternative processes include the fluidized bed reactor developed by REC Silicon [7], the vapour-to-liquid deposition developed by Tokuyama Corporation [8] or the closed loop process adopted by Wacker Polysilicon [9]. Elkem Solar has also developed its own metallurgical refining process, which consists of three main steps, namely 1. slag treatment of the MG-Si, 2. acid leaching, and 3. directional solidification [6]. This process has been the first one to be commercialized and it entered the market in 2009.

Although the energy consumption, and hence the production cost of metallurgically refined Si feedstock, is much lower than the traditional electronic grade (EG) feedstock from the Siemens process, the refining is less effective and the material generally contains higher concentration of impurities, especially of dopants. In particular, the vast majority of the low-cost feedstocks available today contains comparable amounts of both acceptors and donors species, *i.e.* the materials are compensated. Standardization of the content of impurities for these materials has not been agreed upon on a world-wide basis yet; nevertheless attempts have been made at establishing threshold levels of different impurities for these materials. In 2008, a plenary discussion at the 'Arriving at well-founded SoG silicon feedstock specifications' workshop [10], suggested possible specifications for the silicon feedstocks. The acceptable values for the different impurities were set on the basis of their effect on the electronic properties of the material. The general assumption was that the efficiency of the solar cell could be related primarily to the content of impurities, as extensively discussed by Davis *et al.* in [11]. Considering these assumptions and suggested specifications as a starting point, the recently published standard SEMI PV17-0611 has defined acceptable levels of main impurities in silicon feedstock to be used for PV applications [12]. The specifications for the main impurities for representative SoG-Si materials investigated in this work are reported in Table 1.1. As far as the dopants concentrations are concerned, iso-resistivity and iso-yield charts have been worked out for different boron and phosphorus concentrations [13], showing thus which ingot yields and resistivities can be expected as a function of the concentrations of boron and phosphorus in the feedstock.

Table 1.1. Specifications for solar grade silicon (SoG-Si) category IV, as reported in SEMI PV17-0611 [12].

Impurity element	Specification SEMI PV 17-0611, Category IV
B	Target: ≤ 0.380 ppmw Tolerance: ± 0.060 ppmw
P	Target: ≤ 0.790 ppmw Tolerance: ± 0.170 ppmw
C	≤ 43 ppmw
Ti, Cr, Fe, Ni, Cu, Zn, Mo	≤ 0.2 ppmw
Na, K, Ca	≤ 4 ppmw

The evaluation of the acceptable dopants concentrations mentioned above provides a good general indication for the quality of the compensated materials. Nevertheless, it is worth noting that the standard, well-known analytical methods and parameters that have been developed and calculated over the last decades for the assessment of the properties of non-compensated crystalline Si materials might not be applicable to compensated materials in a straightforward way. This is due to the fact that these materials have shown an effect on, for example, the relation between resistivity and the net or total doping level, the increased minority carrier lifetime, the decreased minority carrier mobility, or the slow-down of the

formation rate of the detrimental boron-oxygen complexes. Hence, comprehending the impact of compensation on material properties is of paramount relevance for the full assessment of the compensated metallurgically refined feedstocks as base materials for crystalline silicon solar cells.

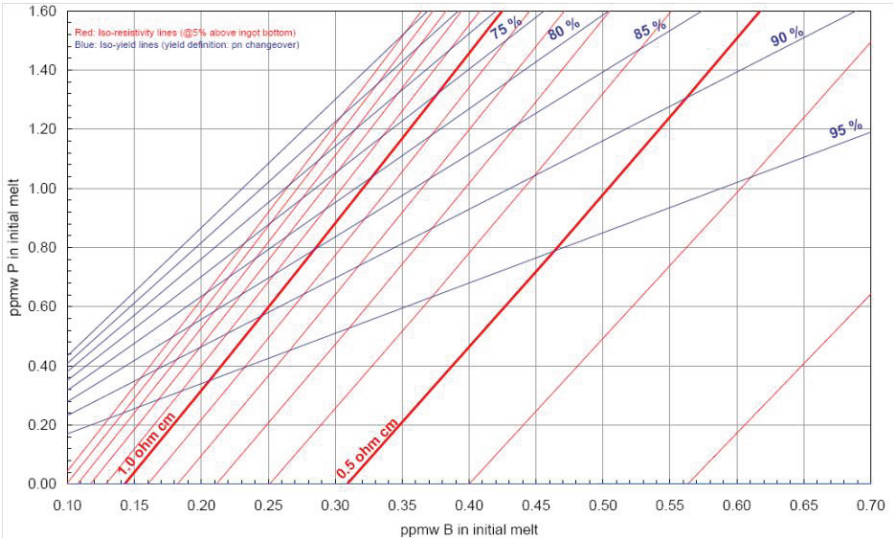

Figure 1.1. Iso-resistivity (red) and iso-yield (blue) lines as a function of the boron and phosphorus concentrations in the feedstock. Reproduced from [13].

The work presented in this thesis focuses on the material-related topics discussed above. Directionally solidified ingots from compensated solar grade Si feedstock of different purities and from poly-Si feedstock have been investigated. The compensated SoG-Si feedstock materials presented here have been produced by Elkem Solar through the proprietary metallurgical refining process mentioned above. The materials were received at NTNU/SINTEF between 2008 and 2011, with a decreasing amount of dopants and other impurities with time thanks to the efforts made for the improvement and control of the refining process [14]. This represents a unique possibility to investigate commercially available materials, where the contaminants are naturally present in the feedstock prior to the final directional solidification and not deliberately added/diffused into the final ingot. This feature allowed relating the effect of compensation to as-grown material properties such as resistivity, minority carrier lifetime, majority carrier mobility, content of and interaction with impurities (*e.g.* oxygen, carbon, and transition metals). Moreover, the production of solar cells from these materials allowed a more thorough evaluation of the mechanisms influencing solar cell performance. Throughout the experimental work carried out in this thesis, a comparison of the material properties of the compensated ingots with reference, non-compensated ingots directionally solidified under similar process conditions was performed. This comparison allowed separating the effect of compensation from other material-related properties, *e.g.* concentration of light elements or metal impurities.

The thesis is based on published and submitted articles. The introduction to the on-going research on compensated crystalline silicon materials, focusing mainly on the effect of B and P as compensating dopants, has the intent of providing a background for the properties

discussed in the articles. The overview of the investigated materials and characterization techniques used in this work is providing experimental details. The discussion part is intended to briefly summarize the contents of the articles. Finally, an outlook suggests possible directions for future investigations on compensation in crystalline SoG-Si materials.

Chapter 2

Compensation in solar grade silicon – an overview

This chapter includes the relevant background for the results presented in this work, with a focus on compensation in multicrystalline silicon (mc-Si). An introduction to compensation and its effects on material properties, the interaction between doping species and the interaction with other main impurities are discussed in the following. The published literature and the results from the present work are discussed concurrently.

2.1 Introduction to compensation

Compensation in a semiconductor material can be defined as the concurrent presence of donor and acceptor species in comparable amounts. Therefore, the majority carrier density in a non-compensated and a compensated p-type semiconductor, *i.e.* hole concentration, can be expressed through the following equations, respectively:

$$p_0 \cong N_A^- \qquad \text{for a non-compensated material} \qquad \text{Eq. (2.1)}$$

$$p_0 \cong N_A^- - N_D^+ \qquad \text{for a compensated material} \qquad \text{Eq. (2.2)}$$

where p_0 is the majority carrier density in a p-type semiconductor (hole concentration), and N_A^- and N_D^+ are the acceptor and donor density, respectively. They will be reported as N_A and N_D in the following.

It is worth noting that the concurrent presence of various acceptor and donor species can lead to an overall compensated mc-Si material. Nevertheless, this work focuses only on boron and phosphorus as acceptor and donor species, respectively. The reason for this is twofold. First, B and P are the two doping species of the highest relevance in the Si solar cells market, due to numerous reasons related to the refining mechanisms in the successive steps of the production processes usually employed. Second, B and P are by far the main doping species present in the materials investigated in this work. Aluminium is an acceptor in silicon semiconductors and it constitutes the third most present doping species in the materials presented here. Its concentration is generally at least one order of magnitude lower than B; hence its role can be safely neglected in the following.

Under the assumptions that:
i) the B and P concentrations in these materials are well below the respective solid solubility limits in silicon (maximum solubility of $1 \cdot 10^{21}$ cm^{-3} at 1420 °C for B and $1.3 \cdot 10^{21}$ cm^{-3} at 1200 °C for P [15], which correspond to 2 at% and 2.6 at%, respectively);
ii) the presence of other doping species or ionized impurities is expected to be negligible when compared to those of B and P,
the acceptor and donor densities for the materials investigated in this work can be approximated with the B and P atomic concentrations, respectively:

$$N_A^- \cong [B] \qquad \text{Eq. (2.3)}$$

$$N_D^+ \cong [P] \qquad \text{Eq. (2.4)}$$

Note that these approximations are valid under the assumption that all dopant atoms are ionized, *i.e.* they fully contribute to the electron and hole densities. This assumption is confirmed to be valid by Voronkov and Falster [16], and is discussed further in Section 2.2.

Therefore, considering Eq.s (2.1) to (2.4), for the materials studied in this work the majority carrier density can be expressed as following:

$$p_0 \cong [B] \qquad \text{for the non-compensated materials} \qquad \text{Eq. (2.5)}$$

$$p_0 \cong [B] - [P] \qquad \text{for the compensated materials} \qquad \text{Eq. (2.6)}$$

This assumption is to be valid throughout this work, unless otherwise specified.

Compensation itself occurs at all times within the p-n junction of a semiconductor, although in this work the discussion is restricted to the compensation which occurs in the bulk of crystalline Si ingots, *i.e.* the material that constitutes the base of silicon solar cells. Moreover, the following is limited to p-type materials.

2.1.1 Principles of compensation

Various expressions have been suggested to define the amount of compensation. One of them is the compensation ratio, R_C [17]. For a p-type material, the compensation ratio is defined as the ratio of the sum of acceptor density, N_A, and donor density, N_D, over their difference:

$$R_C = \frac{N_A + N_D}{N_A - N_D} \qquad \text{Eq. (2.7)}$$

Hence, the R_C values increase with increasing compensation and are greater than unity for compensated materials, *i.e.* $R_C = 1$ for a non-compensated material, whereas $R_C \rightarrow \infty$ for a fully compensated material (*i.e.* $N_D \approx N_A$). A threshold for high compensation is considered to be at $R_C = 3$, *i.e.* $R_C > 3$ for highly compensated samples [18]. This definition of R_C will be

used throughout this work for an evaluation of the degree of compensation in the investigated materials.

Another formula for compensation has been reported by Dubois *et al.* [19] and it defines the compensation level, C_l, as the ratio of the donor density, N_D, over the difference between acceptor and donor densities:

$$C_l = \frac{N_D}{N_A - N_D} \qquad \text{Eq. (2.8)}$$

According to this definition, p-type compensated materials have C_l values that increase with increasing compensation, where 0 is the limit value for a low-compensated material (*i.e.* low donor density) and $C_l \rightarrow \infty$ for a fully compensated material (*i.e.* $N_D \approx N_A$). In contrast to the R_C definition, $C_l = 0$ for a non-compensated p-type material.

In order to define the acceptable doping levels for boron and phosphorus in the compensated (p-type) materials to be used for solar cells, the two main requirements relate to resistivity and ingot yield. Both these parameters depend on the B and P contents in the feedstock, and a general view is that the ingot should have a resistivity range from 1 Ω·cm up to 2-2.5 Ω·cm. For the yield criterion, a compensated ingot should have its upper resistivity limit (*i.e.* 2-2.5 Ω·cm) within the normal top-cut range, which is typically above 90% ingot height. A specification for silicon feedstock for photovoltaics was recently described in the SEMI standard PV17-0611 [12], and the upper limits considered in this standard for the dopants in Category IV are given in Table 2.2 below.

Table 2.2. Upper limits for doping elements in solar grade silicon feedstock as set in standard SEMI PV17-0611, Category IV [12].

Dopant	Upper limits for dopants in SoG-Si - Category IV [6]		
	ppbw	ppba	cm^{-3}
B	380	990	$5.0 \cdot 10^{16}$
P	790	716	$3.5 \cdot 10^{16}$

The feedstock materials investigated in the present work were produced at Elkem Solar in Norway, where the first materials were produced in a pilot line and the last ones in the industrial line. The concentration of both boron and phosphorus decreased over time, and the typical values of the latter are reported in Table 2.3.

Table 2.3. Typical concentrations of boron and phosphorus in Elkem Solar Silicon®, ESS™ [14].

Dopant	Elkem Solar Silicon® - Typical concentrations		
	ppbw	ppba	cm^{-3}
B	220	573	$2.9 \cdot 10^{16}$
P	620	562	$2.7 \cdot 10^{16}$

For comparison, boron specifications for non-compensated mc-Si ingots to be used for solar cell processing are generally in the range 50-150 ppbw (130-390 ppba, $6.5 \cdot 10^{15}$-$1.9 \cdot 10^{16}$ cm^{-3}) [20]. Within these B concentrations, the resistivity of the materials is in the range 0.5-2.0 Ω·cm.

2.1.2 Quantification of doping levels

Different techniques are available to quantify the doping levels in compensated c-Si materials, allowing measurement of p_0, N_A and/or N_D. This section provides a description of the most common techniques used for c-Si materials or that have been specifically developed for compensated c-Si. The use of glow discharge mass spectrometry (GDMS), resistivity and majority carrier mobility to quantify doping levels are discussed in detail in Chapter 3.

2.1.2.1 By Fe-B pairing

This technique was developed by Macdonald *et al.* [21] and it is based on the formation rate of the well-known Fe-acceptor pairing in c-Si. It allows the direct calculation of N_A and the indirect calculation of N_D, *i.e.* not merely of p_0. A more detailed description of the Fe-B pairs kinetics is provided in Section 2.3.2. This technique uses the time constant of the Fe-B pairs association, which can be directly measured, to calculate N_A. N_D is successively calculated from the N_A value, fitting the N_D and hole mobility values in the formula that relates resistivity, carrier mobility and net doping (see Section 2.4.2). The advantage of this method is that the interstitial iron in c-Si materials is always present as a positively charged impurity, and consequently it readily forms pairs with the acceptors present in the material. Moreover, the determination of N_A is independent on the majority carrier mobility, since the Fe-B pairs formation depends on the diffusion of Fe_i atoms and not of B atoms. On the other hand, the calculation of N_D has greater uncertainty as it depends both on the measured resistivity and on the knowledge of the hole mobility. The materials that were measured with this technique had B and P concentrations in the range 800-1600 ppba ($4\text{-}8 \cdot 10^{16}$ cm^{-3}) and 700-900 ppba ($3.5\text{-}4.5 \cdot 10^{16}$ cm^{-3}), respectively.

2.1.2.2 By infrared (IR) spectroscopy

Various methods have been developed for the quantification of dopants in compensated Si materials using infrared absorption, and they differ for the absorption peaks that are used for the analysis.
A first application allows measuring the total concentrations of dopants in compensated Si, *i.e.* [B] and [P] [22]. The absorption peaks of donors and acceptors can be observed separately in an infrared spectrum at low temperature (approximately 15 K) in a sample that is subjected to light. The application of external light to the material is necessary because, under dark conditions, only the non-compensated centres are absorbing infra-red radiation, and hence only the net doping density can be measured [22]. The drawback of this method is that it requires low temperatures and it is well developed for dopant concentrations below 10^{16} cm^{-3} [21], or materials with high resistivity (above 50 Ω·cm). This concentration is appropriate for the materials presented in this work, but is somehow lower than the concentration in the highly compensated SoG-Si materials.

Another application of this technique is available to measure the total B concentration at room temperature for compensated Si with high B concentrations [23]. The peaks of the B isotopes used for the quantification of [B] are located at 620 cm^{-1} and 644 cm^{-1}, and they are typical of compensated materials. The calibration factor for the quantification of the total B concentration can be calculated by comparison of the intensity of the absorption peak with the concentration measured by other techniques, *e.g.* GDMS [23]. The drawback of this technique is that the absorption peaks mentioned above become visible for high B concentrations (generally above 10^{17} cm^{-3}), which is above the concentration normally accepted for compensated SoG-Si feedstock.

A third application consists in the measurement of the free-carrier absorption (FCA) in the FTIR spectrum, and hence it allows the determination of p_0. The method was introduced by Rein *et al*. [24] for compensated Czochraslki (CZ) silicon and a more detailed description is given by Geilker *et al*. [25]. The free carriers absorb light that carries energy lower than the bandgap. Their concentration can be safely assumed to be equal to p_0 in case of complete ionization and in absence of external generation of carriers. This assumption is strongly valid at room temperature, where the FTIR spectrum is collected. The absorption related to the free carriers depends on the wavelength, on p_0 and on the carrier mobility. A reference float zone spectrum is subtracted from the spectrum of a compensated sample and the contribution of other defects (*e.g.* interstitial oxygen and substitutional carbon) is corrected for. Then the absorption due to the free carriers can be quantified, and consequently the net doping density p_0 calculated. The successive steps performed to obtain the FCA spectrum are shown in Figure 2.1.

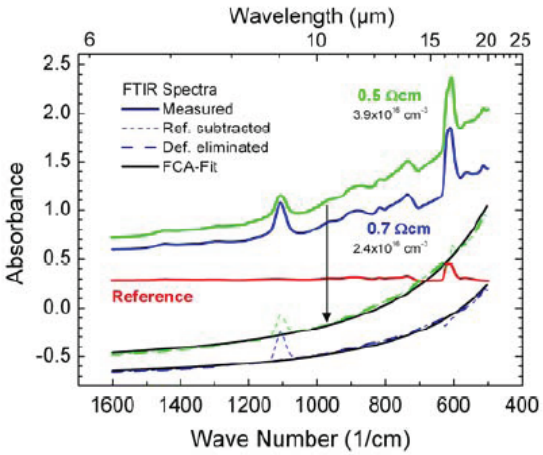

Figure 2.1. Quantification of the free-carrier absorption (FCA). The different subtractions of background and defect absorptions are shown. Reproduced from [25].

2.2 Interaction between main doping species

The concurrent presence of acceptor and donor species in compensated materials can lead to an interaction between them. In particular, evidence of the existence of B-P pairs have been obtained by infra-red spectroscopy measurements [26, 27]. The B and P concentrations investigated in these studies were in the order of 10^{20} cm^{-3} (2-3 at%), a value which is several

orders of magnitude greater than the reasonable concentrations in compensated SoG-Si materials. Consequently their existence in these materials has to be questioned further.

The presence of B-P pairs in compensated SoG-Si was first suggested by Dubois *et al*. [28] as a possible explanation to the reduction of the rate of light induced degradation (LID) due to the formation of boron-oxygen complexes in compensated mc-Si materials compared to non-compensated materials. LID is further described in Section 2.3.1.3, and in this instance it is important to note that the formation of these complexes is believed to occur through diffusion of an oxygen dimer to a boron atom. According to this mechanism, the presence in the lattice of P^+ ions in neighbouring positions to B^- ions causes a screening of the Coulomb field of the B^- ions, which consequently reduces the capture cross section toward the oxygen dimer, or alternatively increases the mean free path for the oxygen dimer to reach a B atom. Hence the diffusion kinetics of the oxygen dimer would be slower compared to non-compensated materials, *i.e.* no screening effect of P^+ ions. A schematic visualization of this mechanism is shown in Figure 2.2.

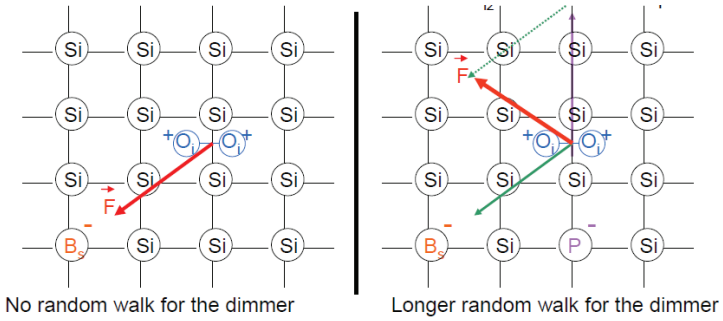

Figure 2.2. Schematic visualization of the suggested mechanism for the slow-down of the B-O complexes formation rate in compensated materials (right) compared to non-compensated (left). The presence of P^+ atoms can increase the random free path for the oxygen dimer to combine with a B^- atom. Reproduced from [29].

The existence of the B-P pairs has been considered in several other studies. Kopecek *et al.* [30] observed LID behaviour in compensated CZ-Si materials and reported an additional peak in photoluminescence (PL) spectra of compensated materials, not seen in the non-compensated ones. This peak increased in intensity with increasing compensation, and it was therefore connected to B-P pairing. More complete PL measurements were reported in a successive study by Peter *et al*. [31] (see Figure 2.3), where it was suggested that also a long-range interaction between B and P, not involving the formation of B-P pairs, could explain the observed peaks. Macdonald *et al*. [32] considered B-P pair formation to explain the dependence of the B-O defect concentration on the net doping content, p_0, and not on the acceptor density N_A, *i.e.* the compensated boron present in the material would not contribute to the formation of B-O complexes because present in a state not reacting with oxygen dimers.

Several other studies have argued the presence of B-P pairs in compensated c-Si materials. Macdonald *et al*. [33] reported their existence to counter the measured majority carrier mobility and the location of the crossover point between Fe_i and Fe-B pairs. More details on

both carrier mobility and Fe-B pairing can be found in the following sections. The authors argue that, if the B-P pairs were present, they would impact the majority carrier mobility due to a reduction of the ionized scattering centres, and the mobility would evidently scale with the net doping density. However, the dependence of majority carrier mobility was observed to be more consistent with the total dopant concentration, *i.e.* N_A+N_D, than with p_0. Moreover, if the B-P pairs were present, they would be expected to form appreciable concentrations of Fe-B-P 'triplets' instead of Fe-B pairs, and a different energy level would be associated with these triplets. In turn, a different location of the crossover point would be observed. However, its location was observed to be similar for compensated and non-compensated materials. Voronkov and Falster [16] concluded that the formation of B-P pairs, if existent, is negligible in compensated CZ-Si materials with doping ranges of practical interest for solar cell applications. They compared the hole density, p, independently measured by light reflection, to the value calculated from the measured resistivity, ρ. They observed that the best agreement between the two values of p occurred for ρ(N*) and μ(N*), where N* = [B]+[P], *i.e.* the B-P pairing is negligible and N_A corresponds to [B]. Moreover, the possible presence of B-P pairs was suggested also in a study on boron-phosphorus compensated n-type material [34]. LID due to the formation of boron-oxygen complexes was observed to occur in this material, which could not have occurred if all the boron were present in B-P pairs.

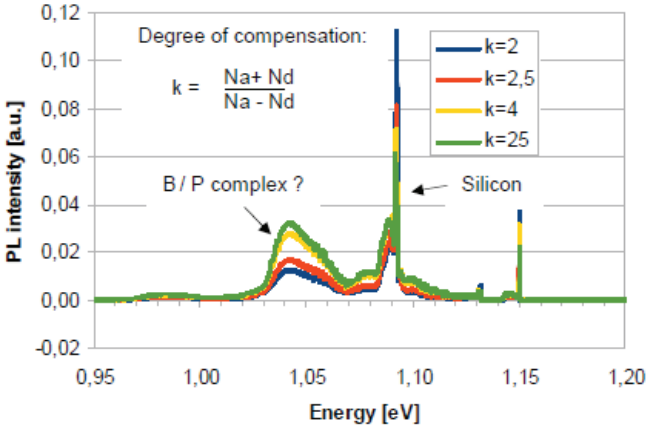

Figure 2.3. Photoluminescence spectra of compensated samples. The peak at ~1.05 eV increases with increasing degree of compensation and it is believed to be connected to B-P interaction. Reproduced from [31].

2.3 Interaction between doping species and main impurities

Directionally solidified mc-Si ingots contain different impurities, which can be present in the material as dissolved atoms, precipitates or clusters. According to their state, these impurities affect material properties to a different degree. Oxygen, transition metals (iron and chromium especially), and carbon are of particular interest in this work, and a description of their effect on material properties in compensated and non-compensated crystalline silicon is made in the following sections.

2.3.1 Oxygen

Oxygen is an impurity not easily removed from directionally solidified mc-Si ingots, due to several reasons. Firstly, the effective segregation coefficient approaches unity [35], and therefore the crystallization does not contribute significantly to its refining. Secondly, the oxygen present in the standard SiO_2 crucibles and crucible coating used for ingot casting diffuses into the Si melt during the solidification process, reacts with the atmosphere in the furnace and eventually contaminates the ingot [36, 37].

Oxygen in crystalline silicon can be present as dissolved atom (single interstitial atom) or as a precipitate. As its effects on material properties differ significantly according to its state, these effects are discussed separately in the following sections.

2.3.1.1 Interstitial oxygen, O_i

Single oxygen atom impurities present in the crystalline silicon material as interstitially dissolved, O_i, are not of major concern; they are considered not to be electrically active and hence not to affect the device performance [38].

The materials presented in this work usually have O_i concentrations in the range 3-12 ppma ($1.5\text{-}6\cdot10^{17}$ cm^{-3}), where the concentration decreases with increasing ingot height (solid fraction). No significant difference in oxygen concentration is observed between ingots cast from compensated SoG-Si feedstock and EG-Si feedstock. These are representative concentrations for the ingots cast in the furnace used in this work [36]. The solid solubility limit of oxygen in silicon is 19 ppma ($9.5\cdot10^{17}$ cm^{-3}) at the temperature reached at the end of ingot solidification [39], and consequently these materials are not expected to have significant concentrations of precipitated oxygen, *i.e.* the solubility limit is generally not reached. This is confirmed by the comparison of interstitial and total oxygen measurements carried out for selected samples in this work. The enhanced oxygen precipitation at grain boundaries and its relation with dislocations in mc-Si materials [40-45] have been studied, but are not further discussed here.

2.3.1.2 Thermal donors, TD, and oxygen-based precipitates

The term *thermal donors* (TD) defines oxygen-based precipitates that are present in crystalline silicon bulk and that affect the electronic properties. They form within specific temperature ranges and contribute to n-type conductivity in the bulk silicon material. Due to this reason they are of greatest concern in p-type materials. Different types of TD have been identified, as reviewed in Ref. [46]. The so-called *old donors* form in the temperature range 350-500 °C and are composed of small clusters of few oxygen atoms, whereas the so-called *new donors* form in the temperature range 650-800 °C and are SiO_2-based precipitates. These complexes can also form during the slow post-solidification cooling of the ingot [38]. The vast majority of the TD that generate in crystalline silicon have O_i as a precursor [38, 47], and hence the formation of TD can be related to the initial O_i concentration, as shown in Figure 2.4. It is observed that the formation rate of the thermal donors within the first 30 min of the annealing increases with increasing O_i concentration [47]. The O_i values reported in Figure 2.4 are representative of CZ-Si materials.

Thermal donors are generally present to a greater degree in monocrystalline silicon (CZ process) than in mc-Si, even though different oxygen precipitates have been observed to occur in significant amounts in mc-Si as well [41, 42]. This is due to the fact that monocrystalline silicon generally contains a higher total oxygen concentration, possibly over the solid solubility limit.

Oxygen precipitates are known to have detrimental effect on minority carrier lifetime [42] and on the performance of the solar cells, as they reduce their conversion efficiency [45, 46, 48]. However, the investigations on compensated SoG-Si materials reported in literature are sparse.

The negligible occurrence of thermal donors and oxygen-based precipitates has been confirmed to be valid for the materials investigated here by the work of Friedl [49] and Gallala [50]. In these two investigations [49, 50], the negligible occurrence of oxygen precipitates has been observed through a 2 hour annealing in Ar atmosphere at 1300 °C, *i.e.* at a temperature above the solid solubility limit for the expected total oxygen concentration, which was performed on several compensated and non-compensated mc-Si materials. Under these annealing conditions, all oxygen precipitates possibly present in the material should have dissolved, and the O_i concentration could be used to estimate the amount of dissolved precipitates. The O_i concentration measured by FTIR after the annealing showed an increase generally well below 1 ppma ($5 \cdot 10^{16}$ cm^{-3}) compared to the as-cast value. This roughly corresponds to less than 10% of the initial concentration, and therefore oxygen-based precipitates are not expected to be present in the as-cast materials studied in this work. Moreover, a second annealing at 500 °C for 2 hours in flushing Ar atmosphere was performed with the aim of obtaining internal gettering. A comparison of the O_i concentration before and after this annealing showed no significant difference, and consequently no formation of TD occurred in these materials. This result is also confirmed by the dependence of the TD formation on the O_i concentration reported above (see Figure 2.4). One can easily observe that for the O_i concentration in the materials reported in the present work, *i.e.* lower than $5 \cdot 10^{15}$ cm^{-3}, the formation of TD after 2 hours of annealing at 450 °C is below $3 \cdot 10^{14}$ cm^{-3} (0.06 ppba).

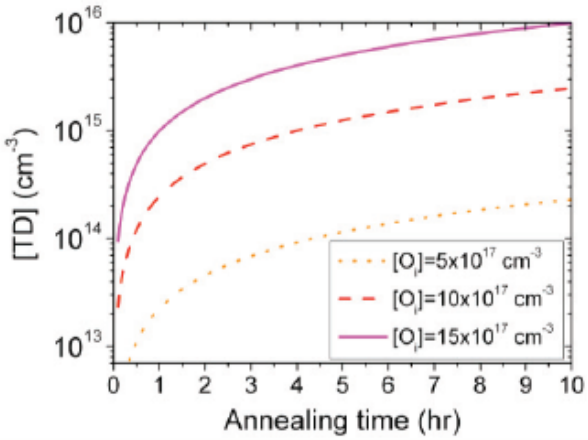

Figure 2.4. Formation rate of TD in CZ-Si as a function of annealing time and initial O_i concentration. Annealing temperature of 450 °C. Reproduced from [47].

These investigations showed no significant difference between compensated and non-compensated materials. Hence, it is safe to assume that compensation does not affect oxygen precipitation for the materials presented here. Nevertheless, as discussed in Section 2.4.3, this is to be considered when relating the resistivity to the doping density.

2.3.1.3 Boron-oxygen complexes

Oxygen impurities in silicon are known to pair up with boron atoms and form boron-oxygen complexes that are responsible for lifetime degradation. These complexes are believed to be the main cause for the lifetime degradation under illumination in B-doped CZ-Si materials [51, 52], with a relative reduction in cell efficiency of up to 10% [53]. These lifetime-limiting complexes are forming in the temperature range 30-130 °C under illumination [51] and they are deep-level recombination centres, localized in CZ-grown materials at E_C - 0.41eV [54], where E_C is the energy level of the conduction band. They are observed in different configurations [55] and they are metastable, where both their formation and annihilation are thermally activated processes [53]. The annihilation occurs by illumination in the temperature range 70-220 °C [56]. The complex concentration has been observed to be proportional to $[O_i]^2$ and linearly proportional to $[B_s]$, and therefore their formation is believed to involve an interstitial oxygen dimer and a substitutional B atom, *i.e.* B_s - O_{i2} [53, 55]. In this prospect, the knowledge of the O_i concentration in the Si material has an important role as it is a precursor of the lifetime-limiting defect formation [47]. More recently, an alternative configuration for these defects has been suggested, based on the degradation characteristics, where an interstitial B atom, B_i, is paired up with an oxygen dimer, *i.e.* B_iO_2 [16]. These lifetime-limiting complexes have been successfully converted into low-recombination active complexes under annealing at high temperature [57]. Such annealing is generally used by the solar cell manufacturers and hence the lifetime degradation might not influence the performance of the solar cell. The possibility of an interaction between TD and the oxygen dimers involved in the formation of the boron-oxygen complexes has been observed by Schmidt and Bothe [53], and is therefore to be taken into account when evaluating the electronic properties of the material. For these EG-Si materials, the boron-oxygen complexes have been observed to be dependent either on the B atom concentration [53] or on the holes concentration, and not the B atom concentration [16].

The occurrence and the kinetics of boron-oxygen complexes have been studied also in compensated c-Si by several researchers. A reduction of the formation kinetics compared to the EG materials has been observed [28]. The interaction between B and P doping species is considered partially responsible for this slow down, together with an uneven spatial distribution of B and P atoms which affects the O_{i2} diffusion and with the reduction in the hole mobility. Under these considerations, the extent to which the lifetime degradation due to the formation of boron-oxygen complexes occurs in compensated mc-Si is much lower than in non-compensated EG-Si. The deactivation rate of these complexes in compensated materials has been reported to be inversely proportional to the total boron concentration and not to be dependent on the net doping density, p_0 [58]. This suggests that boron itself is directly connected to the deactivation mechanism. Moreover, the activation of these complexes was found to depend quadratically on the net doping density, p_0^2, and not on the total boron concentration, N_A [59]. The dependence of the concentration of these complexes on the net doping density, as opposed to the acceptor density, was observed in several other studies [24, 30, 33, 60, 61]. Independently on these trends, it can be observed that compensation itself does not introduce a further lifetime-limiting mechanism compared to B-doped crystalline Si

of similar net doping densities. The dopant concentrations that were generally investigated in the literature are in the range of 2.6-4.4 ppma for [B] and 1.8-2.6 ppma for [P] [28, 59], greatly higher than the concentrations in the materials presented here.

It is worth noting that the extent to which the performance of the materials presented in this work is affected by boron-oxygen complexes is considered to be negligible, *i.e.* overshadowed by the effect of compensation or of metallic impurities. The lifetime degradation due to the formation of the complexes is high for materials which do not contain significant amounts of other lifetime-limiting impurities, *e.g.* metal impurities [52].

2.3.2 Iron

Iron is widely considered as one of the most detrimental impurities in c-Si materials, causing reduction in the solar cell efficiency for concentrations above ~2 ppba (10^{14} cm^{-3}) [11]. Compensated SoG-Si feedstock can contain greater concentrations of several impurities compared to EG-Si feedstock, and iron is among these impurities [19]. Iron is most commonly present in silicon as interstitially dissolved, Fe_i, or in metal-rich precipitates of small dimension and relatively fine distribution [62]. Therefore, compared to other metals with higher solubility and/or diffusivity which can be present in precipitates of a coarser dimension but lower spatial density, iron is generally more detrimental for material properties [62]. It can also be present in the as-grown state paired with acceptor species, *i.e.* in Fe-B pairs. The FeB pairs can split into Fe^{+}_{i} and B^{-}_{s} under illumination, which increases the recombination activity of the defect as Fe_i is associated with an energy level deeper than the one associated with FeB pair [63]. Consequently, the Fe_i defect limits the minority carrier lifetime to a greater extent then FeB pairs and it is more detrimental for solar cell performance. The Fe-B repairing rate is proportional to the acceptor concentration, N_A, *i.e.* B^- [64]. Hence, due to a generally greater concentration of B, the impact of Fe-B interaction in compensated SoG-Si can be expected to be higher. It is worth noting that the possible interaction between FeB pairs and P in compensated materials has been discussed in Section 2.2. A clear correlation between lifetime and iron concentration in mc-Si ingot with 27 ppma ($1.3 \cdot 10^{18}$ cm^{-3}) Fe addition to the melt has been shown by Coletti *et al*. [65], although the Fe_i density was limited to 10% of the total iron concentration. In that study an increased crystal defect concentration was observed, and consequently the effect of iron on material properties is not limited to its dissolved state. However, this concentration is much higher than in the materials studied in the present work, and therefore iron is expected to have a limited contribution. As a reference, the Fe_i measured in CZ-Si ingots cast from feedstock materials similar to those used in this work was below 10^{10} cm^{-3} along all ingot height [66].

The impact of dissolved iron in mc-Si materials can be reduced through tailored post-solidification treatments, which aim at modifying the distribution of iron in the bulk, *i.e.* internal gettering of Fe, or in the P-rich region of the solar cell, *i.e.* external gettering of Fe. The effectiveness of internal gettering treatment on as-grown wafers taken from the deteriorated area of the ingot has been shown by Boulfrad *et al*. [67]. External gettering of mc-Si ingot contaminated with 27 ppma ($1.3 \cdot 10^{18}$ cm^{-3}) Fe in the melt by means of P-diffusion and hydrogenation during cell processing showed an increase in lifetime up to 50 times compared to the as-grown value [65]. More details on gettering and its impact on material properties are discussed in Section 2.4.1.

2.3.3 Chromium

Another transition metal that might be present in greater concentrations in compensated SoG-Si than in EG-Si is chromium [19]. Davis *et al*. [11] reported that Cr concentrations exceeding 10^{14} cm^{-3} (~ 2 ppba) lead to reduction in solar cell efficiency in monocrystalline, non-compensated Si. Nevertheless, Coletti *et al*. [68] reported comparable solar cell efficiencies for mc-Si materials deliberately contaminated with $1.1 \cdot 10^{18}$ cm^{-3} (22 ppma) compared to mc-Si references, for solid fractions between 40% and 70%. Chromium can also be externally gettered by heat treatment, due to heterogeneous precipitation [69].

Similarly to Fe, dissolved chromium is generally present as an interstitial impurity, *i.e.* Cr_i, and it is therefore a fast diffuser. As a donor, under thermal equilibrium conditions Cr_i pairs with acceptors, *i.e.* it forms CrB pairs, which introduce shallow energy levels in the bandgap [70]. As discussed above, FeB pairs dissociate under standard illumination conditions, unlike CrB pairs. The latter are dissociated into Cr_i and B_s under heat treatment at 200 °C, which dissociates the FeB pairs as well. Hence, the impact of Cr on minority carrier lifetime can be distinguished from that of Fe through a comparison of lifetime values after illumination (*i.e.* FeB pairs dissociated), after heat treatment (*i.e.* both FeB and CrB pairs dissociated) and in the dark (*i.e.* no pairs dissociated) [19]. Similarly to the effect reported on FeB pairs, compensation reduces the detrimental effect of Cr on minority carrier lifetime by shifting the Fermi level towards mid bandgap, *i.e.* most of the Cr will remain paired with B and therefore have a lower recombination strength [70]. This increase in minority carrier lifetime with increasing compensation has been computed by Dubois *et al*. [19], where Shockley-Read-Hall statistics are used to calculate the recombination due solely to the interaction of Fe and Cr with B (see Figure 2.5). Computational studies on compensated c-Si solar cells showed that the concentration of CrB pairs should not exceed ~10^{12} cm^{-3} (~1 ppba) in order to have a positive impact on the minority carrier lifetime [71].

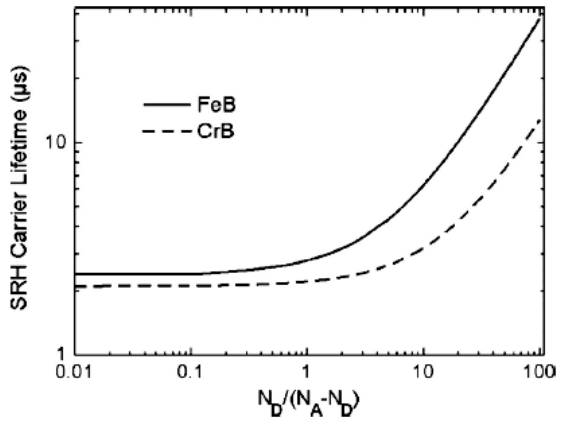

Figure 2.5. Dependence of the minority carrier lifetime on the compensation level. The limitation to lifetime is calculated from Shockley-Read-Hall statistics and is limited to the effect of FeB and CrB pairing. A general increase in minority carrier lifetime with increasing compensation is observed. Reproduced from [19].

The effect of Cr has been investigated for some of the materials presented in this work by Hystad [72]. The comparison of two ingots directionally solidified from similar test materials,

with and without 27 ppma ($1.3 \cdot 10^{18}$ cm^{-3}) Cr addition, allowed studies of the effect of Cr on compensation. The Cr concentrations in the lower part of the ingot were low (units of ppba) due to segregation, but they were already detrimental for minority carrier lifetime, with a reduction of more than one order of magnitude compared to the non-contaminated ingot. On the other hand, after a standard gettering treatment, the lifetime values increased to acceptable levels and solar cells processed from the contaminated material showed no drastic decrease in cell performance. This proves that most of the Cr is present as interstitially dissolved and not strongly segregated at extended defects. Studies of CrB pairs formation in this material confirmed it, as no clear evidence of their existence could be obtained. Similarly to these results, a drastic reduction in minority carrier lifetime and a comparable solar cell efficiency was also observed by Saynova *et al*. [73] in compensated mc-Si ingots deliberately contaminated with 20 ppma (10^{18} cm^{-3}) Cr in the melt and compared to ingots from similar feedstock without Cr addition.

2.3.4 Carbon

Carbon is an impurity generally incorporated in directionally solidified mc-Si materials during crystal growth. Carbon from furnace graphite parts, *e.g.* susceptor and/or insulation, reacts with oxygen in the atmosphere of the furnace to form CO gas [74, 75]. This in turn can dissolve into C and O, and contaminate the Si melt. Moreover, SiO gas evaporating from the melt surface can react with the graphite parts and contaminate the melt as SiC precipitates and CO gas. For this reason, compensated SoG-Si feedstock materials are not expected to introduce a greater C contamination level. Carbon can be present in Si as substitutionally dissolved impurity, C_s, or in precipitates, usually as SiC. Dissolved carbon is not considered detrimental for the electronic properties as it is electrically inactive, whereas SiC precipitates can cause shunting of the semiconductor device. Moreover, SiC precipitates can nucleate in the melt ahead of the solidification front and hence cause growth instabilities and/or constitute nucleation sites for other impurities. Based on a critical review of the solubility values published in the literature, Søiland [74] reported the liquid solubility of carbon at the melting point to be 93 ± 23 ppma ($4.7 \cdot 10^{18} \pm 1.2 \cdot 10^{18}$ cm^{-3}). This is a value well above the levels generally measured in compensated SoG-Si ingots, and also for the materials studied in this work. It is therefore safe to assume that carbon precipitation plays a marginal role in these materials. Nevertheless, carbon plays an important role due to its enhancement of oxygen precipitation, as it constitutes a heterogeneous nucleation site [76]. Moreover, enhanced carbon solubility at extended defects or the presence of nucleation sites, *e.g.* Si_3N_4-based precipitates [77], enhancing the formation of SiC precipitates are relevant in mc-Si materials.

An attempt at evaluating the acceptable C contamination levels in UMG-Si feedstock materials has been reported by Geerligs *et al.* [78]. Multicrystalline Si ingots with addition of 35 ppma ($1.7 \cdot 10^{18}$ cm^{-3}) and 65 ppma ($5.8 \cdot 10^{18}$ cm^{-3}) C to the melt showed solar cell parameters not directly related to the C content. An interaction of SiC with metal precipitates in the neighbourhood was suggested as a possible explanation for the unexpected behaviour of the internal quantum efficiency. High carbon concentrations can also enhance the precipitation of boron at grain boundaries as B-O complexes [43], although the concentrations in that study were greatly higher than those commonly observed in compensated SoG-Si feedstocks. Dubois *et al*. [29] argued that the effect of the interaction between C_s and O_{i2} to form CO complexes in silicon, and consequently its indirect effect on the formation of B-O

complexes, should also be taken into account when evaluating the acceptable C content in compensated SoG-Si feedstock.

2.4 Effect of compensation on electronic properties

Understanding the effect of compensation on the electronic properties is of paramount importance for the overall assessment of compensated solar grade silicon to be used for PV applications. The electronic properties are the most relevant material properties as they are strongly influencing the field performance of the solar cells produced from these feedstock materials. The effect of compensation on the electronic properties of interest in this work is discussed in the following sections.

2.4.1 Minority carrier lifetime

Minority carrier lifetime is related to the carrier diffusion length in a solar cell, and therefore closely related to the cell performance. The effect of single impurities (*e.g.* Fe, O) on lifetime has been discussed in the previous sections, whereas the overall contribution of different impurities in SoG-Si materials and their interaction is discussed in this section.

The bulk minority carrier lifetime in c-Si materials is the overall result of several lifetime-limiting contributions, *e.g.* recombination at metals and at extended defects, or degradation due to acceptor-donor complexes. As discussed above, Fe and O have a detrimental effect on the minority carrier lifetime in p-type c-Si materials due to their interaction with B atoms. Nevertheless, injection-dependent modelling of minority carrier lifetime showed that in practice lifetime is limited also by other mechanisms [79]. That study showed that the lifetime values would be much greater than what generally observed if only the degradation due to Fe and O were occurring. Moreover, the impact of surface recombination is greater for compensated material than for non-compensated material of similar resistivity, *i.e.* the effective lifetime measured in compensated material would be lower [80].

Compensated c-Si materials are generally observed to have lower minority carrier lifetime compared to non-compensated materials of similar net doping (*i.e.* resistivity) [64]. Other than the effect mentioned above, it has been suggested that the high concentration of the minority carrier species, *i.e.* P in the vast majority of p-type compensated SoG-Si, could lead to an appreciable total carrier recombination, even though the recombination mechanism is rather weak in itself [64].

The evolution of minority carrier lifetime with compensation has been computed by Dubois *et al*. [19], through Shockley-Read-Hall statistics at low injection levels. The authors observed that the recombination strength of doping species decreases with increasing compensation. This occurs because the reduction in the free carrier density with increasing compensation, due to the increase in donor density, leads to a shift of the Fermi energy level towards mid-bandgap. This in turn leads to a reduction of the recombination strength of the shallow energy levels, such as those introduced by B neutral atoms. Veirman *et al*. [81] showed that measured effective lifetimes in p-type compensated SoG-Si ingots indeed increase with increasing compensation (see Figure 2.6). The authors modelled the Shockley-Read-Hall lifetime in the

materials, and observed that the increase in P concentration with increasing compensation introduced a defect with a shallow energy level, which excludes any contribution from metals. A similar behaviour has been also reported by Macdonald and Cuevas [82], where the injection-level-dependent Shockley-Read-Hall lifetime due to Fe_i is observed to increase with increasing compensation levels (*i.e.* decreasing net doping). In that study, the increase in lifetime with increasing compensation has been related to deep-energy levels with a wider capture cross-section for minority- than for majority carriers, such as Fe_i in p-type Si. The increase in minority carrier lifetime with increasing compensation was also measured by Peter *et al*. [66] for materials similar to those studied in this work.

As mentioned above, dislocations and extended defects have strong impact on the minority carrier lifetime in mc-Si materials, as they can be recombination active centres [83]. Consequently, compensated SoG-Si materials could affect lifetime through the interaction of dopants with extended defects, *i.e.* by precipitating in electrically active compounds at favourable sites. Boron has been observed to precipitate at grain boundaries in B-O complexes by SIMS measurements [43]. Nevertheless, the B concentration in that study was greatly higher than those for the materials presented in this work, and it is therefore safe to assume that any effect of dopants segregation on carrier lifetime would be negligible in most compensated SoG-Si materials commercially available. This is supported by the fact that, even at the rather low concentrations generally observed in these materials, the electronic properties of the c-Si are limited mainly by metals [11].

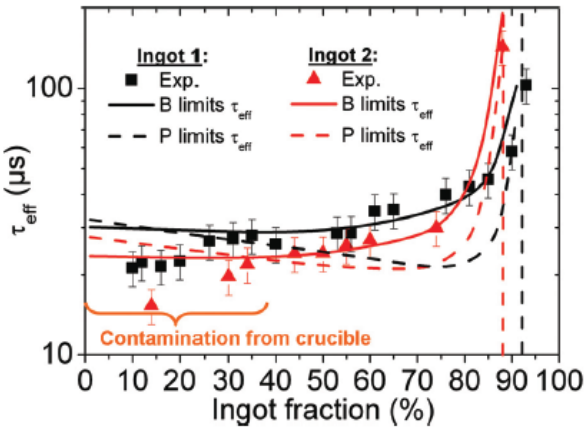

Figure 2.6. Effective lifetime along growth direction for compensated SoG-Si materials. The experimental results are fitted to Shockley-Read-Hall simulations. Reproduced from [81].

The materials studied in this work showed a clear decrease in minority carrier lifetime, with a decrease in the average value at half ingot height by about 50 % for the materials cast from the less clean test compensated SoG-Si feedstock. At this height, the concentrations of the main metal impurities were measured to be similar to the EG-Si references. Consequently, this reduction is believed to be mainly related to the lower resistivity in the compensated samples. Nevertheless, variations in the carrier mobility due to compensation were not taken into account in the measurements and could therefore have influenced the comparison. The effect of compensation on carrier mobility is discussed further in the following section.

Gettering is one of the steps in standard solar cell processing. It can be defined as a three-step process that, without physically removing the unwanted impurities from the bulk material, segregates them into favourable sites with enhanced solubility, thus removing them from the active regions of the device [84]. The impurities are turned into a less harmful state, such as segregated at extended defects or at energetically favourable (precipitation) sites [85], and device performance can be improved. Gettering is particularly effective for metal impurities, provided that they are distributed homogenously over the bulk [84]. For a similar total concentration of metals, their impact on electronic properties is lower when the metals are precipitated at clusters of average bigger size and lower spatial density [62]. This effect has also been observed for materials similar to those presented in this work, where a strong improvement in lifetime was observed after a multi-step gettering involving P-diffusion [85]. The minority carrier lifetime in the compensated SoG-Si samples was improved up to 100 μs after gettering, *i.e.* comparable to the commercial mc-Si reference. For the materials studied in this work, gettering treatments were carried on compensated SoG-Si materials, with and without Cr addition [72]. The average minority carrier lifetime was observed to improve for both types of materials, although the biggest improvement was observed for the Cr-contaminated materials. Similar gettering treatments performed in UMG-Si and compensated SoG-Si materials showed similar lifetime improvements [86, 87].

2.4.2 Majority carrier mobility and density from Hall effect measurements

Carrier mobility determines the manner charge carriers move through a semiconductor under an external electric field [88]. In a semiconductor, the carrier mobility, μ, can be expressed as [89]:

$$\mu = \frac{v_d}{E} \qquad \text{Eq. (2.9)}$$

where v_d is the drift velocity of the charge carrier (*i.e.* the average velocity increase of the carrier between two consecutive collisions caused by the electric field) and E is the external electric field.

Diffusivity of the charge carriers and the carrier mobility are interconnected via the Einstein relation [89]:

$$D_n = \frac{kT}{q}\mu_n \quad \text{for electrons} \qquad \text{Eq. (2.10)}$$

$$D_p = \frac{kT}{q}\mu_p \quad \text{for holes} \qquad \text{Eq. (2.11)}$$

where D_n and D_p are the diffusion coefficients and μ_n and μ_p the mobilities of electrons and holes, respectively; kT/q is the thermal voltage (k is Boltzmann constant, T is the temperature and q is the elementary charge).

The charge carrier diffusivity in turn relates the carrier lifetime in the bulk, τ, to the diffusion length, L, according to the equation [89]:

$$L_n = \sqrt{D_n \cdot \tau_n} \quad \text{for electrons} \qquad \text{Eq. (2.12)}$$

$$L_p = \sqrt{D_p \cdot \tau_p} \quad \text{for holes} \qquad \text{Eq. (2.13)}$$

The diffusion length L is an important parameter for PV solar cells as it indicates the distance the charge carriers travel through the bulk of the solar cell before recombination takes place, and consequently relates to the amount of electric current that can be extracted from the solar cell. Considering Eq. (2.10) to Eq. (2.13), one can observe that the carrier mobility relates to the diffusion length and hence affects the solar cell performance. Carrier mobility itself is affected by both types of doping species in the semiconductor material, and therefore it is essential to understand the effect of compensation on it.

Different carrier scattering mechanisms influence the majority carrier mobility in silicon materials, *e.g.* lattice (phonon) scattering, defect scattering (extended crystal defects, ionized or neutral impurities), and carrier-carrier scattering. The overall carrier mobility, μ_{tot}, that takes into account all these different mechanisms can be approximated through Matthiesen's rule [90]:

$$\frac{1}{\mu_{tot}} = \sum_{i=1}^{n} \frac{1}{\mu_i} \qquad \text{Eq. (2.14)}$$

where μ_i is the mobility related to the i-th scattering mechanism. The balance between these mechanisms varies with temperature, and it has been shown that the dominant scattering mechanisms in a non-compensated CZ-Si material at room temperature are ionized impurity scattering and lattice scattering, as reviewed in [18].

Compared to non-compensated materials of similar resistivity, compensated Si materials have been reported to have lower carrier mobility (at room temperature). As partially reviewed by Rougieux *et al.* [18], this decrease has previously been observed in several studies, with an average reduction of conductivity mobility by about 25% compared to uncompensated samples at similar acceptor density. This reduction has been reported to occur in both mono- and multicrystalline compensated Si materials, but no agreement has been reached yet on the reason behind it. Different mechanisms have been suggested, such as a reduction of the screening effect [18], or a decrease of free carriers that causes a reduced screening of the ionized scattering centres [91], or that compensation could induce fluctuations of the electric potential that cause carrier trapping and introduce deep-level recombination centres within the bandgap [92]. The studies available in the literature have used different techniques to measure or calculate carrier mobility in compensated c-Si, such as Hall effect [17, 23, 60, 81, 92-94], free carrier absorption [25, 32], electrochemical capacitance voltage (ECV) [32, 58, 85, 91, 93, 94] or Fe-acceptor pairing [21]. The reduction in majority carrier mobility has been observed also in this work, where temperature-dependent Hall-effect measurements of compensated samples of different R_C values showed a limited decrease in majority carrier mobility above room temperature, compared to non-compensated references.

The Hall effect refers to the generation of a voltage difference across a semiconductor under the application of external magnetic field and electric current at right vector directions, *i.e.* magnetic field and current are perpendicular, and the voltage thus generated is mutually perpendicular to both of them [90]. The potential difference is referred to as Hall voltage. Hall effect measurements can be carried out on van der Pauw geometry according to the standard ASTM F76-86 [95]. The Hall coefficient, R_H, depends on the Hall voltage, ΔV_H, the applied current, I, the applied magnetic field, B, and the sample thickness, t:

$$R_H = \frac{\Delta V_H}{I}\frac{t}{B} \qquad \text{Eq. (2.15)}$$

where ΔV_H is the potential difference between zero and the applied magnetic field conditions.

R_H relates the conductivity, σ, to the Hall mobility, μ_H [90]:

$$R_H = \frac{r_H \cdot \mu_c}{\sigma} = \frac{\mu_H}{\sigma} \qquad \text{Eq. (2.16)}$$

where r_H is the Hall factor and μ_c is the conductivity mobility. Therefore, the majority carrier mobility is calculated from the measured resistivity, ρ ($\rho = 1/\sigma$), and R_H. The dependence of r_H on carrier compensation is discussed further below.

As mentioned above, the different carrier scattering mechanisms have different relevance at various temperatures. Therefore, temperature-dependent carrier mobility measurements can be used to investigate this balance, and the influence of compensation. The Hall effect measurements carried out in this work allowed comparing the behaviour of the compensated and non-compensated samples over a wide temperature range (70 K to 373 K). It was observed that the compensation-induced reduction of majority carrier mobility at low temperatures compared to the non-compensated references is much more pronounced than at high temperatures (above room temperature). This shows that the contribution from impurity scattering likely increases with decreasing temperature, and that above room temperature lattice scattering dominates over other scattering mechanisms, to the extent that the compensated samples have mobilities much closer to the non-compensated samples. Moreover, the Hall mobility profile for the compensated samples is clearly scaling with the compensation ratio R_C, rather than with the net- or total doping density.

The Hall effect measurements can also be used to calculate the majority carrier density, p, as:

$$p = \frac{1}{q \cdot \rho \cdot \mu_C} = \frac{r_H}{q \cdot \rho \cdot \mu_H} \qquad \text{Eq. (2.17)}$$

For compensated materials, this value corresponds to the net acceptor density, p_0. Eq. (2.17) shows that the calculated p value depends linearly on the value of r_H. The Hall factor is generally constant and considered equal to unity for non-compensated (single doped) materials, *i.e.* the contribution to the carrier mobility is from either electron or holes, whereas for compensated materials it is lower due to the interaction between charge carrier types. The r_H for compensated samples has been reported in the literature with values in the range 0.66 - 0.88 [18, 96], and the value of 0.71 has been presented as an average. This constant value has been used in all the Hall-effect measurements presented in this work, as it has negligible

variations for the compensation levels studied [18] and over temperature. These measurements show that compensation leads to a stronger decrease in majority carrier density with decreasing temperature compared to non-compensated samples. This behaviour is related to both resistivity and mobility, as the increase in resistivity with decreasing temperature is greater for the compensated samples, and the concurrent increase in carrier mobility alone does not fully counterbalance this.

The samples selected for the Hall effect measurements presented in this work were samples with twin boundaries selected from mc-Si ingots. The comparison of the measurements with a CZ-Si reference showed that no contribution from the twin boundaries affected the resistivity and carrier mobility measurements, *i.e.* the behaviour of the samples with twin boundaries resembled that of single crystal samples.

2.4.3 Bulk resistivity

The bulk resistivity of the mc-Si ingots has practical implications for the solar cell processing. For non-compensated c-Si, the optimum bulk resistivity has been empirically determined to be approximately 1 Ω·cm, a value which balances the requirements for carrier recombination, operating voltage of the solar cell and surface passivation [79]. Brody *et al*. [97] modelled the optimal base resistivity for different mc-Si solar cell concepts, and they concluded that for low-bulk-lifetime materials (*i.e.* below 20 μs bulk lifetime) the optimum resistivity value increases with increasing impurity of the bulk material, due to greater dopant-defect interaction. Geerligs and Macdonald [79] have considered the optimal base resistivity due to recombination related to Fe_i and B-O defects (see Figure 2.7), showing that the optimal value increases with increasing defect concentration and it is related to the larger capture cross-section for electrons than for holes in p-type c-Si materials. This finding can be broadly applied to compensated materials. In the industry mc-Si materials with bulk resistivity in the range 1-3 Ω·cm are usually processed.

The vast majority of the compensated solar grade silicon materials available today are produced through directional solidification, where Czochralski and Bridgman/vertical gradient freeze (VGF) techniques are the most used for mono- and multi-crystalline materials, respectively. In directional solidification, one has to consider the segregation profile of the different impurities over solid fraction. In this prospect, the different segregation behaviour of boron and phosphorus impacts on the resulting resistivity profile, which is not constant over the growth direction. The equilibrium segregation coefficient, k_0, of an impurity is defined as the ratio of the concentration in the solid, C_s, over the concentration in the liquid, C_l [98]:

$$k_0 = \frac{C_s}{C_l} \qquad \text{Eq. (2.18)}$$

Boron and phosphorus have different k_0 values, $k_{0,B} = 0.8$ and $k_{0,P} = 0.35$ [99]. The segregation profile along the growth direction can be calculated with Scheil segregation equation [98].

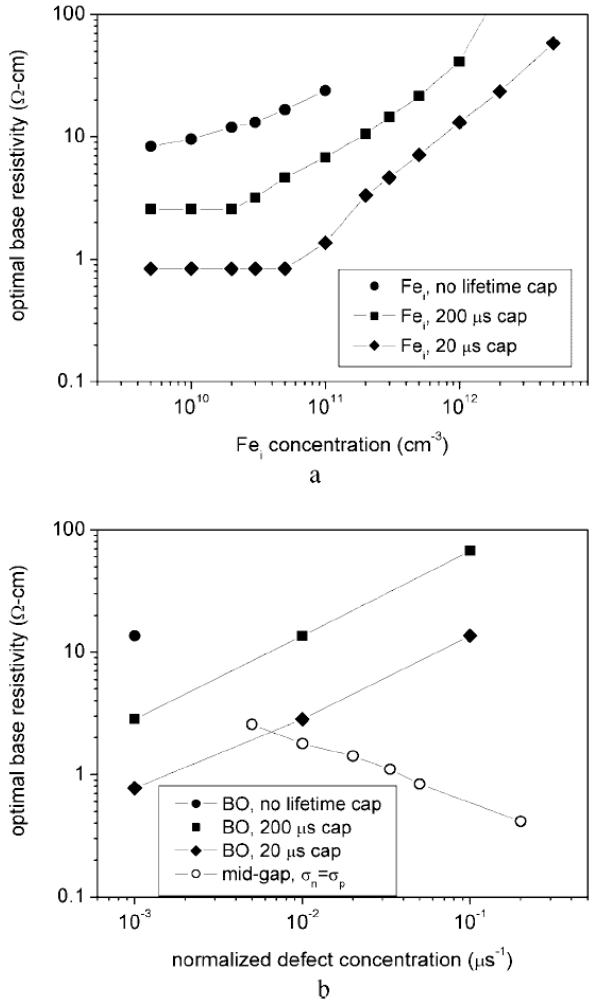

Figure 2.7. Optimal base resistivity calculated as a function of (a) the Fe_i defect concentration and (b) the BO complex concentration. The defect concentration is representative of mc-Si commercial materials. Reproduced from [79].

Hence, by considering the effect of the segregation behaviour and the requirements over the bulk resistivity mentioned above, one can estimate the acceptable resistivity profile along growth direction. Two significant examples are reported below, with R_C values of 10.4 (highly compensated material) and 3.0 (moderately compensated), referred to the dopants concentrations in the melt prior to solidification. The initial concentrations of B and P in the melt are selected according to the criteria considered by Enebakk *et al*. [20], *i.e.* an ingot yield above 90 % and lower resistivity limit of 0.5 Ω·cm for compensated feedstock to be directly used for solidification, and are reported in Table 2.4. Moreover, the initial concentrations are approaching the ones of some of the compensated SoG-Si materials investigated in this work. The segregation profiles of B and P over growth direction for both cases are shown in Figure 2.8, together with the resulting net doping concentration, *i.e.* as the difference between B and P atom concentrations. It can be observed that the highly compensated material reaches the

carrier type transition much earlier than the other material, where the transition occurs at the point where P overcomes B. The presence of the carrier type transition can be observed also in the resistivity profile along the growth direction (see Figure 2.9). The B and P concentrations shown in Figure 2.8 have been used to calculate the resistivity profile using ASTM standard F723-99 [100], under the assumption that the conversion formula could represent the net doping density, *i.e.* [B]-[P] for the p-type region and [P]-[B] for the n-type region. This carrier type transition is not desired in compensated materials, because it decreases the ingot yield, as generally only the p-type part is processed into solar cells. Moreover, as observed in Figure 2.9, the resistivity profile along growth direction increases for the compensated materials, in contrast to the non-compensated EG reference, and at the same time the spread in the values (limited to the p-type region) is rather larger. Consequently, the properties of the material tend to be less homogeneous at the various solid fractions, and this decreases the fraction of the ingot which is suitable for PV processing.

Table 2.4. Initial concentrations of boron and phosphorus in the melt, prior to directional solidification. The R_C value is referred to the melt, *i.e.* null solid fraction.

R_C	Boron- $C_{0,B}$		Phosphorus - $C_{0,P}$	
	ppba	cm^{-3}	ppba	cm^{-3}
$R_C = 10.4$	1430	$7.1 \cdot 10^{19}$	1180	$5.9 \cdot 10^{19}$
$R_C = 3.0$	650	$3.3 \cdot 10^{19}$	325	$1.6 \cdot 10^{19}$

As discussed in Section 2.3.1.2, the possible presence of thermal donors in the bulk crystalline material has to be taken into account when evaluating the resistivity and its relation to the doping density [52]. Nevertheless, as the formation of TD is considered to be negligible in the materials studied in this work, the comparison of the resistivity with the dopants concentration ([B] and [P]), does not introduce significant inaccuracy, *i.e.* no contribution from TD to the n-type conductivity.

2.4.4 Solar cell characteristics

An overview of the effect of compensated SoG-Si feedstock on cell performance and cell processing is presented in this section.

It has been shown that cell parameters of solar cells obtained from compensated CZ-Si ingots of different compensation levels/purity in the feedstock are strongly dependent on the net doping, p_0 [24]. This occurs as net doping influences the resistivity, which in turn influences the open circuit voltage, V_{oc}, and thus the cell efficiency, η. Moreover, a relation between the short circuit current density, J_{sc}, and p_0 has been observed in UMG-Si materials, where the increase in J_{sc} at the top of the ingot compared to the centre part has been related to the lower carrier recombination, in turn related to the lower net doping [86]. However, this behaviour has also been related to the decrease in the minority carrier mobility rather than to the net doping density [81]. The authors measured carrier mobility, cell characteristics and minority carrier lifetime in compensated mc-Si ingots, and observed that the decrease in J_{sc} at high compensation levels could be due to a decrease in minority carrier mobility, to an extent high enough to overbalance the increase in lifetime, *i.e.* the diffusion length would be decreasing with increasing compensation.

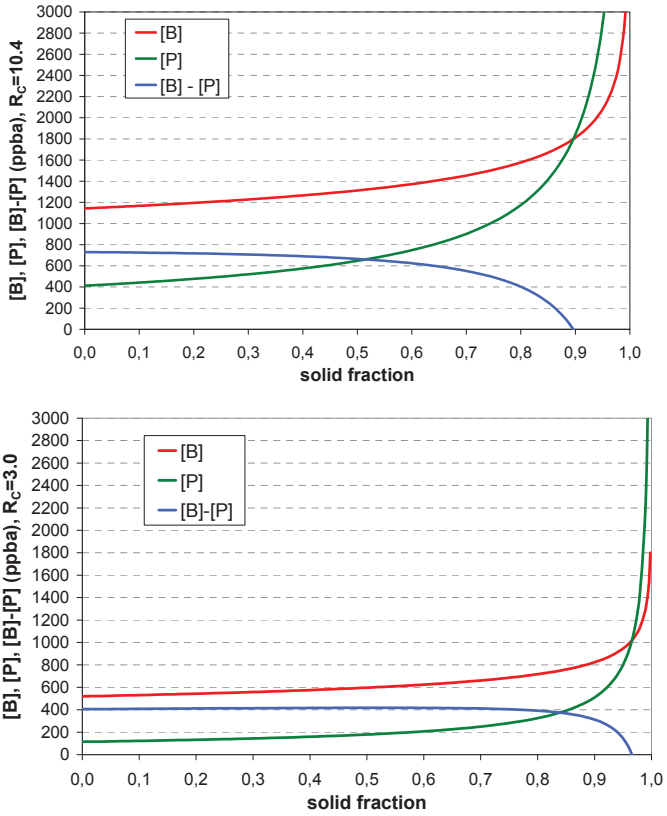

Figure 2.8. Segregation profile of dopants along solid fraction calculated with Scheil equation, initial concentrations in the melt: (above) according to the maximum acceptable for direct use of the compensated SoG-Si feedstock [20], with R_C=10.4; (below) according to acceptable range for SoG-Si feedstock [20], with R_C= 3.

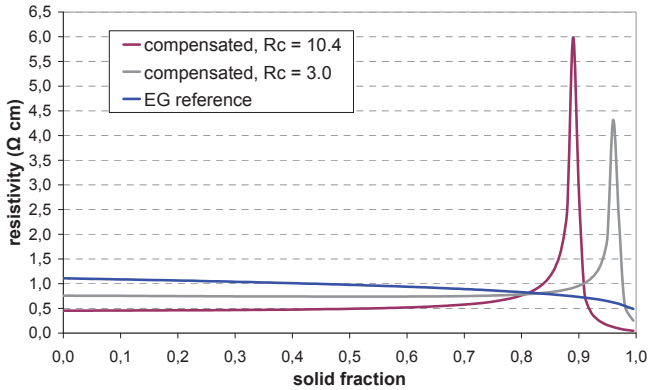

Figure 2.9. Resistivity profile along solid fraction. Calculated from the net doping concentration in Figure 2.8 and ASTM F723-99 [100]. The peak for the compensated materials corresponds to the carrier type transition, where the region on the left is p-type, the region on the right is n-type.

Solar cell processing for the highly doped compensated materials (*i.e.* low resistivity) needs to be modified compared to the standard cell processing. This is due to the fact that the net acceptor concentration of the base requires to be offset by the heavily n-type doped emitter [101], which is done by the standard P-diffusion step in solar cell processing. Therefore, the thickness of the emitter for compensated materials should increase with decreasing base resistivity. In order to obtain these conditions for the emitter, compensated SoG-Si materials should undergo a higher temperature and longer time for the emitter diffusion heat treatment [101].

Other than dopants, compensated silicon materials are generally thought to have greater concentrations of other impurities, especially transition metals, *e.g.* Fe, Ti, Cr, Ni and Cu, are of particular interest due to their influence on the electrical properties. The direct correlation between impurity concentration and impact on device performance has been recently addressed by Coletti [102]. As shown by Buonassisi *et al*. [103], the impact of metals strongly depends on their chemical nature and spatial distribution over the bulk of the wafer. This, in turn, depends on several factors related to growth conditions, grain orientation and post-solidification treatment. As a general distinction, impurities with low solubility and low diffusivity tend to be more detrimental for cell performance as they tend to form more finely distributed precipitates and, if present as point defects, they also introduce deep-level recombination centres [62]. The presence of recombination-active metal precipitates in UMG-Si based solar cells has also been identified as the source for current breakdown [104]. Moreover, the cell performance of directionally solidified B-doped c-Si materials with addition of different metal impurities, such as Fe, Ti, Cu, showed a direct dependence on the total concentration as predicted through the Scheil segregation equation along the growth direction [68]. As discussed in Section 2.4.1, the impact of metal impurities on electronic properties can be lowered through gettering treatments. This effect can easily explain the behaviour of SoG-Si wafers, whose electronic properties are improved during solar cell processing. The impact of grain boundaries on performance of mc-Si solar cells have been modelled by Kassis and Saad [105], who showed that recombination at grain boundaries is one of the dominant mechanisms influencing I-V curves in mc-Si solar cells, especially at low illumination. This simulation is valid only on a general basis, as it does not take into account any effect of grain orientation, *i.e.* it does not consider the enhanced metal precipitation observed at high angle random grain boundaries [103].

An attempt at relating the solar cell efficiency to specific impurities in the bulk material was made by Geerligs *et al*. [78]. The authors modelled the solar cell efficiency reduction due to specific impurities in a UMG-Si feedstock, under the assumption of an inversely linear dependence of minority carrier lifetime on the impurity concentration (see Figure 2.10). The modelled values show a significant impact of Ti (on carrier recombination) and Al (on dopant segregation). In the same study, a 20 % relative reduction in cell efficiency was measured for materials cast from UMG-Si with addition of 5.9 ppma ($2.9 \cdot 10^{17}$ cm^{-3}) Ti, 8.0 ppma ($4.0 \cdot 10^{17}$ cm^{-3}) Fe and 117 ppma ($5.8 \cdot 10^{17}$ cm^{-3}) C to the melt, and compared to reference mc-Si materials. The reduction was primarily due to the high concentration of Ti, with limited contribution from Fe. It is worth noting that these concentrations are greatly higher than the values generally observed in compensated feedstock materials.

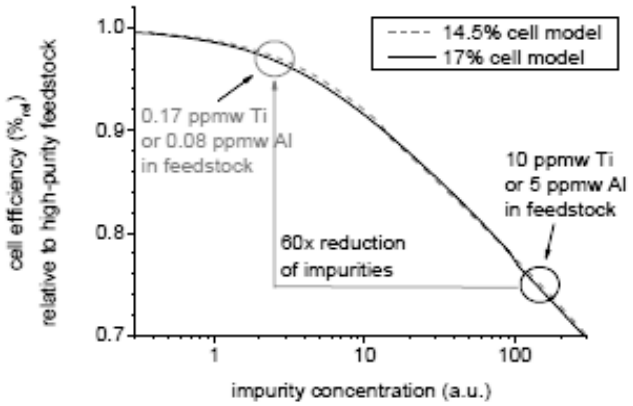

Figure 2.10. Modelled cell efficiency reduction in mc-Si solar cells with impurity concentration. The reference is a high-purity mc-Si cell. Ti and Al are the main impurities considered, under the assumption of carrier lifetime scaling inversely with impurity concentration. Reproduced from [78].

In the present work wafers from compensated materials with various R_C, [B] and [P] were processed into solar cells under a standard process. The solar cells were produced at the International Solar Energy Research Center (ISC), Konstanz (Germany), and more details about the processing steps used for the materials in this work are reported in Ref. [30]. For the ingots with the highest dopants concentrations (1260 ppba B and 762 ppba P in the melt), the maximum cell efficiency and fill factor are 15.5% and 78%, respectively. These values are comparable to the maximum obtained for the reference EG-Si ingots, even though the as-grown lifetime in the compensated ingot was greatly lower. Mc-Si solar cells processed from feedstock materials similar to those used in the present work showed maximum cell efficiency of 16.8%, thus comparable to standard non-compensated mc-Si solar cells [66]. These results confirm that gettering occurs during cell processing for these compensated materials, where the metals, possibly present, change their status into a less recombination-active one, *i.e.* precipitated. Hence, the total concentration of metals is of less importance than their spatial distribution and chemical status. As mentioned above, this gettering was proven to be particularly effective for the compensated material with Cr addition. Similar cell improvements have also been observed by Saynova *et al*. [73] in Cr-contaminated mc-Si solar cells.

Chapter 3

Experimental work and characterization techniques

This chapter provides a description of the materials investigated in this work and of the main characterization techniques used.

3.1 Castings

Several ingots were directionally solidified in a lab-scale Bridgman furnace, Crystalox DS 250 at SINTEF/NTNU. A detailed description of the furnace and the solidification process can be found in reference [106]. The ingots weighed 12 kg and were cylindrical (250 mm diameter and approximately 105 mm height). The majority of the ingots were solidified under standard conditions for the furnace used in this work [106], otherwise any modifications in the process parameters are reported in the articles. An overview of all the ingots, including the feedstock and crucible materials that were used, is shown in Table 3.1. The compensated SoG-Si feedstock was produced through the Elkem Solar metallurgical refining process mentioned above. Note that the feedstock used for ingots ES1, ES2 and MH2 was produced in Elkem Solar lab/pilot line and not in the industrial factory since this feedstock was delivered in 2008 before the factory was finished. The feedstock used for ES3 was produced in the industrial line; in particular the dopant levels were reduced during the last years. A Cr addition of 50 ppmw ($1.3 \cdot 10^{18}$ cm^{-3}) was deliberately added to the Si charge prior to casting of ingot MH2, with the aim of investigating its effect on the material properties. The poly-Si feedstock used in all the remaining ingots was produced through the standard Siemens process, and 128 ppbw of B ($1.6 \cdot 10^{16}$ cm^{-3}) were added to the Si charge with the aim of obtaining a resistivity of 1.0 Ω·cm at 50 % ingot height.

3.2 Material characterization

Each ingot was cut according to the cutting plan sketched in Figure 3.1. Four blocks, named Q1 to Q4, were cut close to the centre of the ingot. Each block was 50x50 mm in cross section. Generally, block Q1 was wafered and processed into solar cells, block Q2 was used for chemical analysis, and block Q3 was wafered and used for Hall mobility measurements, among others. The central slice was used for oxygen- and carbon measurements, whereas side slices were used for lifetime measurements. A short description about the characterization techniques and the parameters used during the measurements are reported in the following sections.

Table 3.1. Overview of the ingots investigated. Feedstock and crucible materials for each ingot are reported.

Ingot name	Feedstock material	Crucible material	Feedstock delivery (year / production)	Ingot casting
ES1 - A1	compensated SoG-Si	SiO_2	2008 lab/pilot	lab/pilot scale
ES2 - A2	compensated SoG-Si	SiO_2	2008 lab/pilot	lab/pilot scale
ES3 - A3	compensated SoG-Si	SiO_2	2010 industrial line	lab/pilot scale
MH2 -M2	compensated SoG-Si + Cr add.	SiO_2	2008 lab/pilot	lab/pilot scale
S1	compensated SoG-Si	Si_3N_4	2008 lab/pilot	lab/pilot scale
R5	poly-Si	SiO_2	N/A	lab/pilot scale
R6	poly-Si	SiO_2	N/A	lab/pilot scale
Cru1R - P1R	poly-Si	Si_3N_4	N/A	lab/pilot scale
CruP1 - P1	poly-Si	Si_3N_4	N/A	lab/pilot scale
CruP4 - P4	poly-Si	Si_3N_4	N/A	lab/pilot scale
CruP5 - P5	poly-Si	Si_3N_4	N/A	lab/pilot scale

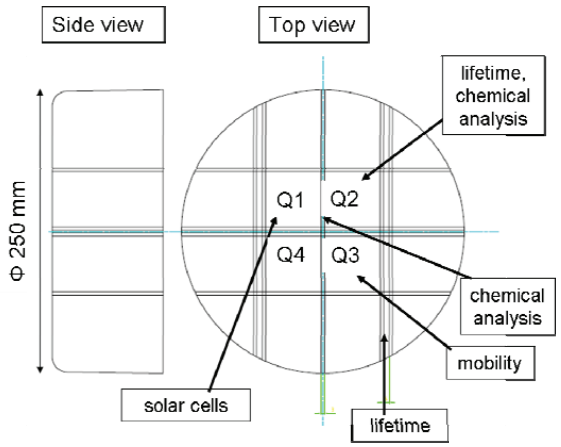

Figure 3.1. Side view (left) and top view (right) of an ingot. The cutting plan is shown, with a description of the various characterizations carried out on the different areas.

3.2.1 Resistivity

The bulk resistivity of the samples was measured with a JANDEL linear four-point probe (FPP) apparatus. The operating principle is shown in Figure 3.2. The four tips are connected to the sample, a constant current is applied through the external electrodes (number 1 and 4 in the figure) and the voltage difference is measured between the internal electrodes (number 2 and 3 in the figure).

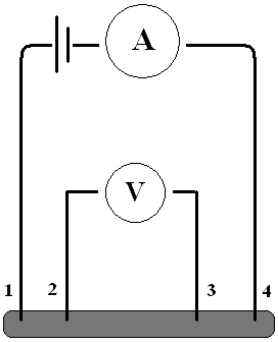

Figure 3.2. Schematic of the four point probe measurements. Electrodes 1, 2, 3 and 4 are all physically connected to the sample, and current is supplied through electrodes 1 and 4, whereas the potential difference is measured between electrodes 2 and 3. Reproduced from [107].

For thick samples, *i.e.* thickness >> 2 mm, the bulk resistivity, ρ, is calculated using the following formula:

$$\rho = 2 \cdot \pi \cdot s \cdot \frac{V}{I} \qquad \text{Eq. (3.1)}$$

where *s* is the distance between the electrodes (0.635 mm in this work), *V* is the mean measured voltage and *I* is the applied current. The measured voltage is averaged over forward and reverse voltage, in order to rule out any asymmetric behaviour in the current path. The applied current was usually set to 500 μA in order to increase the sensitivity for samples with low resistivity. All resistivity measurements presented in this work were carried out on thick samples.

Resistivity measurements were further used to calculate the dopant concentration in the samples, through ASTM standard F723-99 [100]. Under the assumptions considered in this standard, the measured resistivity ρ (in Ω·cm) in B-doped, p-type crystalline silicon materials can be converted into a boron concentration N_B (in cm^{-3}) according to the following empirical equation:

$$N_B = \frac{1.330 \times 10^{16}}{\rho} + \frac{1.082 \times 10^{17}}{\rho\left[1 + (54.56\rho)^{1.105}\right]} \qquad \text{Eq. (3.2)}$$

Hence, an increase in resistivity reflects a decrease in the net doping density, as expected. It is worth noting that the formula used in ASTM F723-99 does not allow a separate calculation of acceptor and donor concentrations, as for compensated materials similar net doping densities (and so resistivities) can be obtained from various combinations of N_A and N_D values [80].

3.2.2 Chemical analyses

Due to the different feedstock materials used in this work, measurements of the chemical composition were given particular focus in order to establish the concentrations of dopants and various harmful impurities. Glow discharge mass spectrometry (GDMS) and Fourier-transform infra-red spectroscopy (FTIR) were the main analysis techniques employed.

3.2.2.1 Glow discharge mass spectrometry (GDMS)

A Thermo Scientific Element GD instrument [108] was used in this work. The operating principles for the glow discharge source and the mass spectrometer are shown in Figure 3.3 and Figure 3.4, respectively. The glow discharge is established by applying a potential difference between the anode and the cathode (the sample) in a closed system flushed with pure Ar gas at low pressure. The surface of the sample is therefore sputtered by the incoming Ar ions, with the neutral sputtered atoms being ionized in the plasma. The ionized atoms are subsequently extracted through the cone and are accelerated towards the magnet. The high magnetic field allows separation of the various ions according to their m/q ratio, where m is the mass and q is the electric charge. The ions are finally counted by detectors. The mass resolution of the instrument used in this work goes down to 0.2 amu (atomic mass units), and the detection limits are generally in the order of tenths of ppbw [109]. The analysed area has a diameter of approximately 8 mm, thus providing a good average bulk concentration for the impurities.

The major advantage of the GDMS instrument is the capability to quantify a large number of elements during a single analysis, while at the same time allowing for low detection limits.

A semi-quantitative analysis of the concentration of the ion, C*, can be carried out as the ion beam ratio, IBR, as defined in the following equation:

$$C^* = IBR = \frac{I_I / A_I}{I_B / A_B} \qquad \text{Eq. (3.3)}$$

where I_I and I_B are the intensities in cps (counts per second) of the impurity isotope (*i.e.* ion) and Si isotope (*i.e.* beam), respectively; A_I and A_B are the relative abundances of the isotopes, as a fraction of the naturally occurring isotopes. Note that the Si isotope used for all calculations is ^{28}Si, which has an abundance of 92.2%, well above the two other Si isotopes, ^{29}Si and ^{30}Si, which have 4.7% and 3.1% abundance, respectively. On a general basis, the isotopes chosen for the analysis are the ones to provide the best trade-off between a high abundance and a low interference with other isotopes or molecules, thus allowing for a lower detection limit.

The quantitative analysis requires the knowledge of the relative sensitivity factor, RSF. This factor expresses the capability of the mass detector to analyse isotopes with different atomic mass units and is, therefore, unique for each isotope and each matrix element for the given instrument. RSF's for several impurities in silicon matrix have been determined for the instrument used in this work and are reported in reference [109]. RSF's values are also dependent on the tuning conditions during the analysis, which were maintained as close as

possible to the reference values in order to avoid any instrument-related error in the quantification.

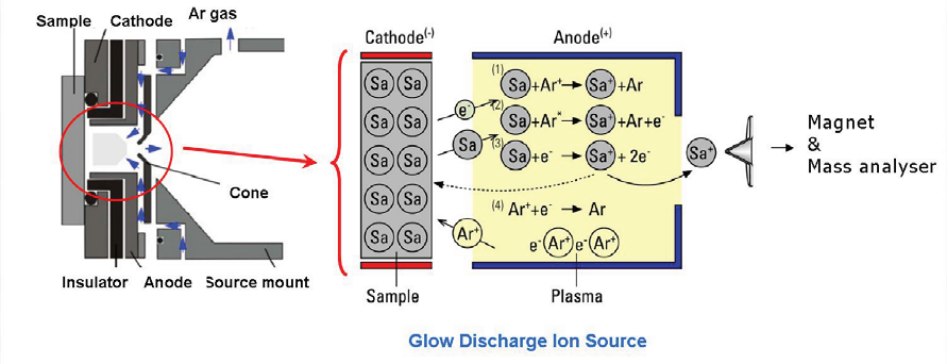

Figure 3.3. Schematic of the glow discharge operating principle. Reproduced from [110].

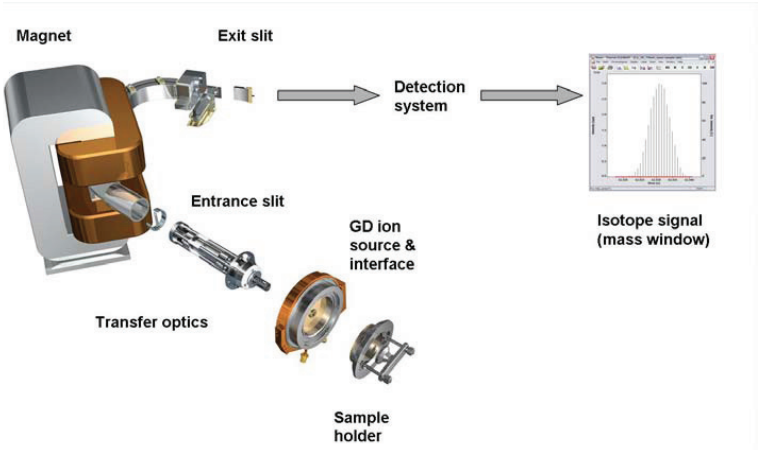

Figure 3.4. Main components of the glow discharge mass spectrometer. Modified from [110].

The concentration of the impurities, C_I, in the samples were hence quantified using the following formula:

$$C_I\left(\text{ppbw}\right) = 10^9 \cdot \text{IBR} \cdot \text{RSF}_I \qquad \text{Eq. (3.4)}$$

Through out this work, the quantification of impurities was performed manually, with a peak-by-peak evaluation of the resulting signals. The peaks of each analysed isotope were compared to a Si sample, deliberately contaminated with several impurities of interest for PV silicon, thus used as reference, and analysed in the GDMS under similar conditions for the investigated samples. This allowed univocally locating the position of the given isotope, *i.e.* no confusion between isotopes and interference peaks. This comparison becomes particularly relevant for isotopes that are approaching the detection limit for the instrument, as in this case the background noise can significantly alter the measured signal intensity.

In this work, the GDMS instrument was used to quantify dopant concentrations (B and P), and main metal impurities (*e.g.* Al, Ti, Cr and Fe). The possibility to use GDMS measurements to establish the net doping density has been argued to be too unreliable, especially for high compensation levels [32]. Nevertheless, in this work the total concentrations of both B and P have been measured by GDMS, while the net doping density, p_0, has been calculated from the measured resistivity using ASTM standard F723-99, as discussed in Section 3.2.1. This value has been compared to the net density as measured by GDMS, i.e. [B]-[P], and the deviation between these two techniques was observed to be within the error of the measurements. Hence, for the relative low dopant concentrations in the compensated materials studied in this work the difference in the total concentrations of B and P corresponds closely to p_0.

Concentration profiles along ingot height were obtained, and a comparison with the equilibrium Scheil segregation profile was carried out in order to evaluate the measured concentrations. A 10 min pre-sputtering was used in all analyses, thus avoiding the effect from possible surface contamination. The sputtering rate in the analysis of silicon samples is assumed to be approximately 1 µm/min.

3.2.2.2 Fourier transform infra-red spectroscopy (FTIR)

A Thermo Scientific Nicolet 6700 FT-IR spectrometer [111] was used in this work. The operating principle of an infra-red spectrometer is based on the fact that, at these wavelengths (*i.e.* 2.5-25 µm), the atomic bonds in molecules are excited and absorb energy through vibration at specific wavelengths. These wavelengths therefore constitute the fingerprint of the given atomic bond, as they can be generally univocally associated to a specific atomic bond. A (near-) infrared laser passes through the silicon sample and the outgoing interferogram is measured by a detector on the other side. The absorption spectrum is then calculated through a fast Fourier transform and used for the quantification. A simplified layout of an FTIR spectrometer is shown in Figure 3.5.

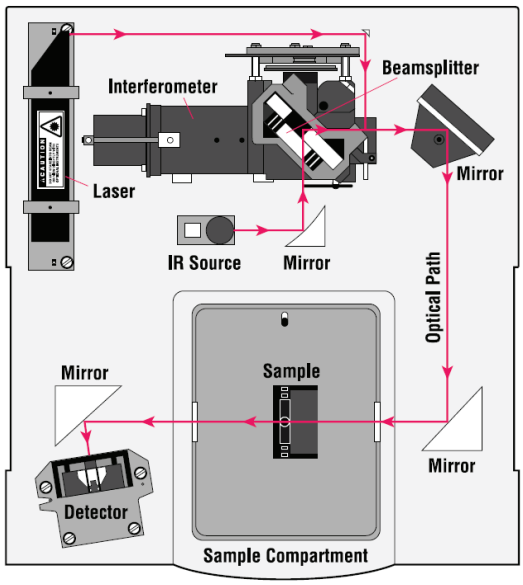

Figure 3.5. Simplified layout of an FT-IR spectrometer. Reproduced from [112].

Transmittance, T, is more frequently used instead of measured absorbance, A, in the quantification of the concentration of the molecule. Transmittance is defined as:

$$T = \frac{I_S}{I_B} = e^{a \cdot t \cdot c} \qquad \text{Eq. (3.5)}$$

where I_s is the intensity of the light transmitted through the sample, I_B is the intensity of the incoming light (*i.e.* background), a is the molar absorptivity, t is the thickness of the sample (defined as the optical path travelled by the incoming light), and c is the concentration of the species.

The FTIR measurements presented in this work were carried out at room temperature. Under these conditions, interstitial oxygen, O_i, and substitutional carbon, C_s, can be quantified, and their absorption peaks are centred at 1107 cm^{-1} and at 605 cm^{-1}, respectively. A typical spectrum recorded for the samples studied in this work is shown in Figure 3.6. Note that the two spectra reported in the figure are from two heights in the same ingot and hence differ in resistivity. Thus they show that an increased scattering occurs at low energy (*i.e.* low wavenumber region). In order to limit the contribution from the noise due to low resistivity, a higher number of scans was used for samples with low resistivity, *i.e.* primarily the ingots from the compensated SoG-Si feedstock. The number of scans was 64 for the higher resistivity samples and 128 for the lower resistivity samples. Nevertheless, it is worth noting that a higher dopant concentration, especially in compensated samples, introduces a further source of uncertainty in the carbon measurements that ought to be taken into account. The detection limit for oxygen in float zone silicon samples can be estimated to 1 ppma, whereas the detection limit for mc-Si samples and especially for compensated mc-Si samples is somewhat higher.

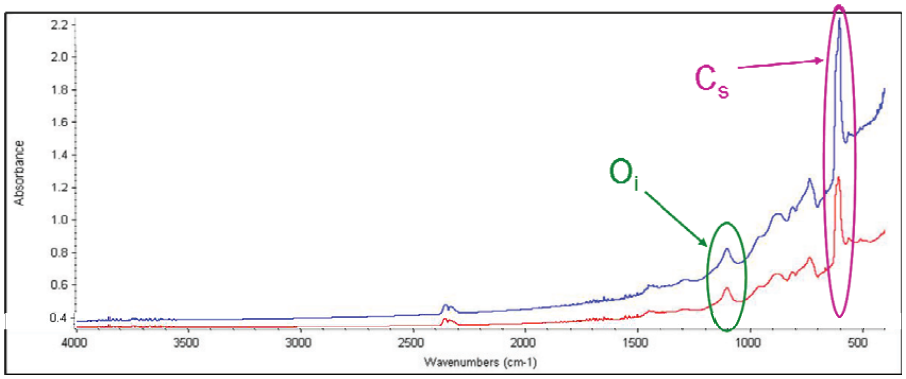

Figure 3.6. Typical FTIR spectrum for the samples investigated in this work. Two spectra from different heights of ingot R6 are shown, the red spectrum has higher resistivity (lower ingot height). The O_i and C_s peaks are centred at 1107 cm^{-1} and 605 cm^{-1}, respectively.

Different international standards provide various calibration factors that relate the measured transmittance to the concentration of interstitial oxygen and substitutional carbon in a crystalline silicon material. The measurements reported in this work were quantified using SEMI standard MF1188 [113] for O_i and MF1391 [114] for C_s. The resolution was set to 4 cm^{-1}.

3.2.3 Minority carrier lifetime

Minority carrier lifetime in a semiconductor is defined as the average time required for an excited minority carrier to recombine [115]. Various recombination mechanisms are contributing to the recombination rate of minority carriers in crystalline silicon, such as radiative recombination, Auger recombination, recombination through traps and surface recombination [116].

Carrier lifetime is an important property to measure in silicon for PV applications because it is closely related to the solar cell performance. Different established techniques are available for measuring minority carrier lifetime in crystalline silicon materials for PV applications, both in the steady-state and in the non-steady-state (transient) conditions. Steady-state conditions are satisfied when the generation rate and the recombination rate for the charge carriers are in balance, *i.e.* lifetime can be determined for a given carrier injection level. Under non-steady-state conditions the injection level is time dependent and lifetime can be determined through the measured time decay constant. In this work, two measuring techniques were mostly used, namely quasi-steady-state photoconductance decay (QSSPC) and microwave photoconductance decay (μw-PCD). Their operating principles and measuring parameters are described in the following sections. A comparison of different techniques to measure minority carrier lifetime and of their advantages and disadvantages is found in [83].

3.2.3.1 Quasi-steady-state photoconductance decay (QSSPC)

This technique measures the minority carrier lifetime as a function of carrier injection level [117].

Under steady-state illumination, the generation rate of electron-hole pairs in a semiconductor is in balance with the recombination rate. This can be expressed as current densities:

$$J_{ph} = J_{rec} \qquad \text{Eq. (3.6)}$$

where J_{ph} and J_{rec} are the current densities due to photogeneration and recombination, respectively.

J_{ph} can be then expressed as a function of the excess minority carrier density, Δn, and of the effective minority carrier lifetime, τ_{eff}:

$$J_{ph} = \frac{\Delta n \cdot q \cdot W}{\tau_{eff}} \qquad \text{Eq. (3.7)}$$

where q is the electric charge and W is the thickness of the sample.

Under steady-state illumination conditions, the change in the photoconductance, $\Delta\sigma_L$, in a sample of thickness W can be expressed as:

$$\Delta\sigma_L = q \cdot W \cdot \left(\mu_n + \mu_p\right) \cdot \Delta n \qquad \text{Eq. (3.8)}$$

where q is the electric charge, μ_n and μ_p are the mobilities of electrons and holes, respectively, and Δn is the excess carrier density averaged over the sample thickness. For silicon semiconductors, electron and hole mobilities as a function of the excess carrier densities are well known.

Consequently, for a given Δn, the effective minority carrier lifetime, combining Eqs. (3.7) and (3.8), can be expressed as [117]:

$$\tau_{eff} = \frac{\sigma_L}{J_{ph} \cdot \left(\mu_n + \mu_p\right)} \qquad \text{Eq. (3.9)}$$

In a QSSPC instrument, a silicon sample is subjected to a light pulse, where the variation in the light source intensity is much slower than the effective lifetime of the sample, *i.e.* the excess electrons and holes generated by the light source have time to relax back to equilibrium concentrations. Hence, the steady-state conditions are approached at all times due to the slow decaying intensity of the light source. A coil connected to the sample allows measuring the decay over time in the photoconductance of the sample. The minority carrier lifetime is then determined via means of Eq. (3.9).

The measurements presented in this work were carried out on a WCT-100 photoconductance tool from Sinton Consulting Inc. The size of the coil is approximately 25 mm in diameter, therefore the measurements are averaged over a wide area. The spatial resolution is hence limited by the size of the coil connected to the sample. The measured samples were blocks, *i.e.* the thickness was well above 10 mm in order to avoid any contribution from the back-surface scattering. The surface was ground down to 1200 SiC grit size, thus any light scattering effect due to surface roughness was reduced. As the samples were not passivated, the effective lifetime determined according to Eq. (3.9) was corrected for the surface recombination. This correction is performed automatically in the software operating the instrument, which runs a PC1D simulation described in [118]. The injection level for the measurements reported in this work was 10^{15} cm^{-3}, a value widely used in literature for p-type, mc-Si materials. The values are averaged over 5 repetitions.

3.2.3.2 Microwave photoconductance decay (μw-PCD)

This technique is a non-steady-state method that measures the time constant of the decay in conductivity of a sample illuminated by a short and intense light pulse. It allows fast lifetime scans on the samples. The spatial resolution is limited by the size of the laser source.

Carriers are introduced in the sample through a laser pulse. A microwave antenna emits a microwave signal towards the sample, and the signal is reflected back by the sample. The microwave antenna measures the decay over time of the reflected signal, which depends on the conductivity of the sample. The minority carrier lifetime, τ, is calculated from the measured conductivity decay, σ_{ph}, which follows an exponential behaviour and can be expressed as:

$$\sigma_{ph} = k \cdot e^{-t/\tau} \qquad \text{Eq. (3.10)}$$

where k is a constant, t is the time and τ is the effective lifetime.

The signal reflected back from the sample to the microwave antenna generally comes from an area of the sample wider than the pulsed laser, especially for laser spot size << 1 mm^2. This contributes to a reduction in the signal-to-noise ratio, and the lateral resolution is increased by acquiring repeated measurements from the same spot.

A Semilab Microwave Photo Current Decay WT-200 Wafer Scanner instrument was used in the measurements reported in this work. The measurements were performed at the Institute for Energy Technology (IFE) in Oslo and the parameters are reported in Table 3.1. Each pixel in the lifetime maps reported in this work is an average of 16 measurements. The lifetime maps are reported with a colour scale representing 80 % of the measurements, *i.e.* the remaining 20 % of the measured values are either below the minimum or above the maximum in the map. The samples were passivated and the preparation procedure is reported in Table 3.2. The surface recombination effects are strongly decreased through the passivation of the sample surface. Therefore, the contribution from surface recombination can be overlooked and the μw-PCD lifetime maps reported in this work are dominated by bulk lifetime.

Table 3.1. Parameters for the μw-PCD measurements.

Spot size (excited area)	1 mm^2
Resolution in X-Y mapping	500 μm
Laser pulse duration	200 ns
Laser penetration depth	30 μm
Laser frequency	10.4 GHz
Laser wavelength	904 nm
Number of repetitions	16

Table 3.2. Sample preparation for μw-PCD measurements. Courtesy of IFE.

Step #	**Treatment**	**Purpose**
1	Chemical polishing - CP5	Removal of organics
2	Etching in HF	Removal of contaminations
3	Piranha solution	Cleaning
4	HF etch	Removal of surface oxides
5	a-Si:H layer deposition	Deposition of the passivation layer
6	annealing	Stabilization of passivation layer
7	μw-PCD measurement	-

3.2.4 Hall mobility

Carrier mobility in crystalline silicon for PV applications is of great interest due to its correlation with minority carrier lifetime and, consequently, with solar cell performance. Moreover, the effect of compensation on the scattering mechanisms influencing carrier mobility has not been fully understood yet, and especially its temperature dependence. Various techniques have been developed to measure carrier mobility, either conductivity mobility or Hall effect mobility. This section will focus on the latter.

The Hall effect in a semiconductor sample consists in the generation of a potential difference across the semiconductor under an external magnetic field applied at given angle to the applied electric current; the electric field generating the potential difference is perpendicular to both the current and the magnetic field vectors [90]. The potential difference is defined as the Hall voltage, V_H, and can be expressed as following:

$$V_H = \frac{R_H \cdot I \cdot B}{t} \qquad \text{Eq. (3.11)}$$

where R_H is the Hall coefficient, I is the applied electric current, B is the applied magnetic field, and t is the sample thickness. For a p-type, uncompensated material, the Hall coefficient is defined as:

$$R_H = -\frac{r_p}{pq} \qquad \text{Eq. (3.12)}$$

where r_p is the Hall factor, which is constant and generally assumed to be equal to unity under high field conditions [90]. p and q are the acceptor density and electric charge, respectively.

Furthermore, the conductivity σ can be expressed as $\sigma = \mu_c \cdot N \cdot q$, where μ_c is the conductivity mobility and N is the carrier density. Hence, the Hall coefficient can be formulated as:

$$R_H = -\frac{r_p \times \mu_C}{\sigma} \qquad \text{Eq. (3.13)}$$

and consequently the Hall mobility, μ_H, can be related to the conductivity mobility, μ_C, through the Hall factor, r_p:

$$\mu_H = r_p \cdot \mu_C \qquad \text{Eq. (3.14)}$$

The temperature-dependent Hall effect measurements reported in this work were carried out on square samples of 9x9 mm^2 size, laser cut from bigger wafers. Aluminium contacts were evaporated at the corners of the sample, and a short annealing at 400 °C was carried out to stabilize the ohmic contacts between the deposited Al layer and the bulk of the Si samples. The van der Pauw geometry was adopted [119]. The setup for the instrument and the quantification of the measured material properties were carried out according to ASTM standard F76-86 [95]. First resistivity was measured under no-field conditions, then the value of the R_H coefficient was calculated from the measured Hall voltages under the applied magnetic field, and consequently it was possible to calculate the majority carrier mobility. For

this purpose, the simplifying assumption of a Hall factor constant and equal to unity was considered. Finally, majority carrier density was calculated from the measured resistivity and Hall mobility.

3.2.5 Solar cell properties

The three parameters that are widely used to characterize the performance of a solar cell are the short-circuit current density, J_{sc}, the open-circuit voltage, V_{oc}, and the fill factor, FF [116].

The short-circuit current density, J_{sc}, is ideally equal to the light generated current density, J_L [116]. J_{sc} can be expressed as follows, under the approximation of a constant generation rate of electron-hole pairs, G:

$$J_{SC} = J_L = q \cdot G \cdot \left(L_e + W + L_h \right) \qquad \text{Eq. (3.15)}$$

where q is the electric charge, W is the thickness of the depletion region and L_e and L_h are the diffusion lengths of electrons and holes, respectively.

The open circuit voltage V_{oc} is then expressed as:

$$V_{OC} = \frac{kT}{q} = \ln\left(\frac{I_L}{I_0} + 1 \right) \qquad \text{Eq. (3.16)}$$

where I_L and I_0 are the light generated current and the saturation current, respectively.

The fill factor, FF, is a parameter that measures how close to the ideal conditions the solar cell is operating and is defined as following:

$$FF = \frac{V_m \cdot I_m}{V_{SC} \cdot I_{SC}} \qquad \text{Eq. (3.17)}$$

where V_m and I_m are the voltage and the current at the maximum power output, respectively. The maximum power output (*i.e.* $P_m = V_m \cdot I_m$) is also defined as the optimum operating load.

The conversion efficiency of the solar cell, η, can be then defined as a function of the three parameters described above:

$$\eta = \frac{P_m}{P_{in}} = \frac{V_{OC} \cdot I_{SC} \cdot FF}{P_{in}} \qquad \text{Eq. (3.18)}$$

where P_m is the power at the operating point and P_{in} is the total power in the incident light.

The solar cell processing and the determination of the current-voltage characteristics presented in this work were performed at International Solar Energy Research Center (ISC) Konstanz, Germany. The processed wafers were 50 x 50 mm^2, a non-standard size for the cell processing. The cell size and the fact that cells from different ingots were processed in

different batches ought to be taken into account when comparing the solar cells from wafers of the various ingots. In particular, the reproducibility of the various steps in the processing, *e.g.* edge isolation, is a clear source of scattering in the results. Standard, mc-Si wafers of known cell properties were cut down to the same size and processed in the same batch along with the materials presented here, with the aim at discerning the effect of cell processing from the material properties. The solar cell processing sequence used here was adapted from the standard sequence reported in reference [30]. Current-voltage characteristics were measured under standard illumination conditions (1.5 AM). J_{sc}, V_{oc}, η and FF values are reported in this work.

Chapter 4

Summary of the publications

The main results of the articles included in this work are presented in this chapter.

4.1 Compensation in SoG-Si

Articles 1, 2 and 3 report on compensation in solar grade silicon and the resulting material properties.

The aim of *Article 1* was to evaluate the impact of compensated SoG-Si feedstock on bulk and cell properties, and therefore its suitability for solar cell applications. This was performed through comparison of two compensated ingots with two reference ingots, cast under similar conditions from EG-Si feedstock. Hence differences in materials properties could be related primarily to the feedstock, although the cast-to-cast variability is to be considered as well. The compensated ingots had initial dopant concentrations which lead to a lower base resistivity until the semiconductor type transition, *i.e.* above 90 % ingot height. Lower effective minority carrier lifetime was measured and this could be due to the combined contribution of compensation and of higher concentration of recombination active impurities, *e.g.* transition metals. Nevertheless, the measured concentrations of main metal species (*i.e.* Al, Ti, Fe) at 50% ingot height approached the detection limits for the GDMS instrument. The dissolved oxygen concentration was comparable to the reference materials, whereas the dissolved carbon concentration was significantly higher and showed significant differences between the parallel ingots. It is worth noting that the dissolved carbon was measured by FTIR and consequently increased scattering and uncertainty in the measurements on the compensated materials is expected due to lower resistivity and hence greater free carrier absorption. Solar cells were processed and showed comparable efficiency, with maximum value of 15.5%. The strong improvement in the performance of the material during cell processing could mean that gettering occurred to a great extent in the compensated materials.

The purpose of *Article 2* was to provide a novel and simple method to measure the net doping density in compensated materials. International standards are available for the conversion between resistivity and doping density for non-compensated materials. In this article, the standard ASTM F723-99 was applied to compensated materials for the quantification of the net doping density, *i.e.* N_A-N_D. This was compared to the net dopant concentration as measured by glow discharge mass spectrometry (GDMS). The comparison was done under the assumption of full ionization of the doping species present in the material. This assumption has been found to be valid for the dopant concentrations in the materials studied

in the present work. The deviation between the net doping density calculated from the measured resistivity and measured by GDMS showed no significant difference between compensated and reference materials. Impurities, such as oxygen or metals present in different concentrations in the materials, are known to lead to electrically active atoms and/or complexes. No clear evidence of such electrically active species was observed among the investigated materials.

The objective of *Article 3* was to study the impact of compensation on majority carrier mobility and majority carrier density. Hall-effect measurements were performed on samples with different degrees of compensation and/or different concentrations of acceptor and donor species, and compared to reference materials. The measurements were carried out over a broad temperature range, in order to distinguish the contribution from the two main carrier scattering mechanisms, *i.e.* ionized impurity scattering and lattice scattering. The mobilities were observed to increase with decreasing temperature for both materials. It was concluded that the contribution from ionized impurity scattering has a strong effect at low temperature (<150 K), where the increase in majority carrier mobility compared to room temperature is 2 to 5 times lower for the compensated materials. At high temperatures (>250 K), lattice scattering was confirmed to be the main scattering mechanisms, and the difference between the compensated materials and the references is small. In particular, the sample with the lowest degree of compensation showed comparable mobility. The temperature profile of the majority carrier mobility showed a dependence on the compensation ratio R_C, where the mobility increase with decreasing temperature is more pronounced for the materials with low R_C.

4.2 Silicon nitride crucibles

The scope of *Article 4* was to investigate the effect of silicon nitride (Si_3N_4) crucible materials on bulk properties of the grown ingots. Silicon nitride crucibles are an alternative to the widely used silica crucibles for directional solidification of mc-Si ingots due to the possibility of reusability for successive castings (re-runs), and consequently of a lower cost of the solidification step. The different thermal properties of the Si_3N_4 crucibles lead to different melting temperature for the Si charge and a possible furnace modification for obtaining standard casting conditions was discussed. Another potential advantage of the Si_3N_4 crucibles is the absence of a contamination source for oxygen compared to silica crucibles. It was shown that, with the coating concept employed in this study, this advantage could not be utilized. In order to avoid sticking of the ingot to the crucible walls, the Si_3N_4 crucible coating layer required to be oxidized and, consequently, oxygen contamination of the ingot occurred through reaction between the melt and the coating. Moreover, it was shown that the oxygen concentration depended primarily on the melting temperature and the coating firing temperature. Unwanted boron and phosphorus contamination of the melt due to reaction with the crucible occurred during the high temperature steps. The boron contamination was eliminated through the selection of pure raw materials for the production of the crucibles. The phosphorus contamination was strongly reduced within few re-runs of the crucibles.

4.3 Impact of Cr in compensated SoG-Si

Article 5 focused on the impact of chromium on the bulk and electronic properties of compensated solar grade silicon. Two parallel multicrystalline ingots directionally solidified from similar feedstock, with and without 27 ppma ($1.3 \cdot 10^{18}$ cm^{-3}) Cr addition to the SoG-Si charge, were studied. Chromium is a detrimental impurity in crystalline Si, both in the dissolved and in the precipitated state. When present in the dissolved state, Cr introduces a deep level in the band gap and, hence, leads to carrier recombination and lifetime degradation. Cr-rich precipitates can also be electrically active and limit minority carrier lifetime. In this study it was shown that the Cr addition caused a significant decrease in the as-grown minority carrier lifetime, and its values were below the detection limit of the mw-PCD instrument used. Nevertheless, a lifetime improvement of 2 orders of magnitude was obtained after a P-diffusion step, which showed that for this material external gettering is likely occurring. This diffusion step was similar to the step commonly used during solar cell processing, and solar cells showed efficiencies approaching the undoped reference ingot. Consequently, it was concluded that good solar cells could be produced at high levels of chromium contamination. Moreover, the effective segregation coefficient for Cr was calculated from the measured concentrations along the growth direction. The calculated value was observed to be approximately 40 times higher than the reported equilibrium value.

Chapter 5

Further work

The majority of the characterization techniques and standards widely used today for silicon for solar cells have been developed and optimized for electronic grade, non-compensated materials. It is therefore extremely important to develop tools and procedures for compensated materials, as this would allow a more meaningful comparison with reference materials and a more precise determination of the compensation related effects.

In the recent years, several studies have been dedicated to the manner specific impurities and/or defects in compensated materials are behaving compared to non-compensated references, *e.g.* B-O complex or carrier mobility. A big challenge would be to assess the contribution of various impurity and defect sources on the overall performance of the material. For example how ingot growth parameters, doping species content, metal impurities content or extended defect density, interact with each other. In this manner, one could obtain a better understanding of the main mechanisms that dominate the performance in a compensated material.

The majority carrier mobility presented in this work showed how the contributions from different carrier scattering mechanisms over a wide range of temperature are influenced by compensation. Nevertheless, minority carrier mobility should be measured as well in order to get a better understanding of the behaviour of compensated SoG-Si solar panels in the field. This is due to the fact that minority carrier mobility influences minority carrier diffusivity. This in turn relates to minority carrier lifetime, which is the bulk property that is widely used to evaluate the material quality of crystalline silicon for solar cells.

The compensated SoG-Si materials investigated in this work showed higher dissolved carbon concentration than the reference EG-Si materials, as measured by FTIR. Due to the higher doping density, the increased free carrier absorption increases the signal-to-noise ratio and hence the accuracy of the measurements can be questioned. Understanding the accuracy is important with relation to the presence of silicon carbide precipitates. They can be detrimental for solar cell performance since they might cause shunting when located across the p-n junction. Moreover, since cast-to-cast variations have been observed for both the reference and the compensated materials, it is important to understand how the greater scattering in the dissolved carbon concentration measurements in the compensated materials is dependent on the feedstock and/or the process conditions (*e.g.* nucleation phase and reactions with furnace atmosphere).

The advantages related to the use of silicon nitride crucibles over the widely used silica crucibles are limited by the requirements related to the chemistry of the crucible coating layer.

The coating concept used in this work has shown not to be favourable for low oxygen contamination of the Si ingot. Hence, the development of new coating concepts which allow obtaining easy ingot release, crucible reusability and low oxygen contamination at the same time could provide the necessary input for a wide adoption of these crucibles materials.

References

[1] Worldwide electricity production from renewable energy resources, in: 12th inventory - Edition 2010, Observ'ER, Paris (France), 2010.
[2] G. Hering, Year of the tiger, in: Photon International - The solar power magazine, 3 (2011) 186-218.
[3] European Commission, A Strategic Research Agenda for Photovoltaic Solar Energy Technology, 2007.
[4] J. Siemer, Breaking the €1 barrier, in: PHOTON International - The solar power magazine, 7 (2011) 122-127.
[5] J. Herron, Return to the oligopoly?, in: PHOTON International - The solar power magazine, 5 (2011) 192-198.
[6] J.O. Odden, G. Halvorsen, H. Rong, R. Gløckner, Comparison of the energy consumption in different production processes for solar grade silicon, in: Silicon for the Chemical Industry IX, Oslo (Norway), 2008.
[7] http://www.recgroup.com/en/tech/FBR/, last accessed: December 2011.
[8] A.F.B. Braga, S.P. Moreira, P.R. Zampieri, J.M. Bacchin, P.R. Mei, New processes for the production of solar-grade polycrystalline silicon: A review, Solar Energy Materials & Solar Cells, 92 (2008) 418-424.
[9] E. Schindlbeck, Wacker polysilicon, in: Alternative Energies Conference, Paris (France), 2007.
[10] Plenary discussion, Arriving at well-founded SoG silicon feedstock specifications, Amsterdam (Netherlands), 2008.
[11] J.R. Davis, A. Rohatgi, R.H. Hopkins, P.D. Blais, P. Rai-Choudhury, J.R. McCormick, H.C. Mollenkopf, Impurities in silicon solar cells, IEEE Transactions on electron devices, 27 (1980) 677-687.
[12] SEMI PV17-0611 - Specification for Virgin Silicon Feedstock Materials for Photovotaic Applications, 2011.
[13] S. Grandum, A.-K. Søiland, E. Enebakk, K. Friestad, Requirements to compensated SoG Si for high performance solar cells, in: 4th Crystalline Silicon Solar Cells Workshop, Taipei (Taiwan), 2010.
[14] A.-K. Søiland, K. Peter, P. Preis, R. Søndenå, I. Odland, E. Enebakk, R. Tronstad, Investigation of Cz-monocrystals, p- and n-type, produced from 50/50 mix of Elkem Solar Silicon® and polysilicon, in: 5th Crystallline Silicon Solar Cells Workshop, Boston (USA), 2011.
[15] F.A. Trumbore, Solid solubilities of impurity elements in germanium and silicon, Bell System Technical Journal, 3 (1960) 205-233.
[16] V.V. Voronkov, R. Falster, Latent complexes of interstitial boron and oxygen dimers as a reason for degradation of silicon-based solar cells, Journal of Applied Physics, 107 (2010) 053509.
[17] J. Libal, S. Novaglia, M. Acciarri, S. Binetti, R. Petres, J. Arumughan, R. Kopecek, A. Prokopenko, Effect of compensation and of metallic impurities on the electrical properties of Cz-grown solar grade silicon, Journal Applied Physics, 104 (2008) 104507.

[18] F.E. Rougieux, D. Macdonald, A. Cuevas, Transport properties of p-type compensated silicon at room temperature, Progress in Photovoltaics: Research and Applications, 19 (2011) 787-793.
[19] S. Dubois, N. Enjalbert, J.P. Garandet, Effects of the compensation level on the carrier lifetime of crystalline silicon, Applied Physics Letters, 93 (2008) 032114.
[20] E. Enebakk, A.-K. Søiland, J. Håkedal, R. Tronstad, Dopant specification of compensated silicon for solar cells of equal efficiency and yield as standard solar cells, in: 3rd Crystalline Silicon Solar Cells Workshop, Trondheim (Norway), 2009.
[21] D. Macdonald, A. Cuevas, L. Geerligs, Measuring dopant concentrations in compensated p-type crystalline silicon via iron-acceptor pairing, Applied Physics Letters, 92 (2008) 202119.
[22] B. Kolbesen, Simultaneos determination of the total content of boron and phosphorous in high-resistivity silicon by ir spectroscopy at low temperatures, Applied Physics Letters, 27 (1975) 353-355.
[23] R. Zierer, G. Gartner, H.J. Möller, Determination of dopant concentration in UMG-silicon by FT-IR spectroscopy, Hall- and resistivity measurements, in: Proceedings of 25th European Photovoltaic Solar Energy Conference, Valencia (Spain), 2010, pp. 1318-1321.
[24] S. Rein, W. Kwapil, J. Geilker, G. Emanuel, M. Spitz, I. Reis, A. Weil, D. Biro, M. Glatthaar, A.-K. Søiland, E. Enebakk, R. Tronstad, Impact of compensated solar-grade silicon on Czochralski silicon wafers and solar cells, in: Proceedings of 24th European Photovoltaic Solar Energy Conference, Hamburg (Germany), 2009, pp. 1140-1147.
[25] J. Geilker, W. Kwapil, I. Reis, S. Rein, Doping concentration and mobility in compensated material: comparison of different determination methods, in: Proceedings of 25th European Photovoltaic Solar Energy Conference, Valencia (Spain), 2010, pp. 1322-1327.
[26] R.C. Newman, R.S. Smith, Local mode absorption from boron arsenic and boron phosphorus pairs in silicon, Solid State Communications, 5 (1967) 723-726.
[27] V. Tsvetov, W. Allred, W.G. Spitzer, Localized vibrational modes in silicon: B-P pair bands, Applied Physics Letters, 10 (1967) 326-329.
[28] S. Dubois, N. Enjalbert, J.P. Garandet, Slow down of the light-induced degradation in compensated solar-grade multicrystalline silicon, Applied Physics Letters, 93 (2008) 103510.
[29] S. Dubois, N. Enjalbert, J.P. Garandet, Specific kinetics and amplitude of the light-induced-degradation in strongly compensated solar-grade multicrystalline silicon solar cells, in: Arriving at well-founded SoG silicon feestock specifications, Amsterdam (Netherlands), 2008.
[30] R. Kopecek, J. Arumughan, K. Peter, E.A. Good, J. Libal, M. Acciarri, S. Binetti, Crystalline Si solar cells from compensated material: behaviour of light induced degradation, in: Proceedings of 23rd European Photovoltaic Solar Energy Conference, Valencia (Spain), 2008, pp. 1855-1858.
[31] K. Peter, R. Kopecek, E. Enebakk, A.-K. Søiland, S. Grandum, Towards 17% efficient multicrystalline solar grade silicon solar cells, in: Proceedings of 25th European Photovoltaic Solar Energy Conference, Valencia (Spain), 2010, pp. 2607-2611.
[32] D. Macdonald, F. Rougieux, A. Cuevas, B. Lim, J. Schmidt, M. Di Sabatino, L.J. Geerligs, Light-induced boron-oxygen defect generation in compensated p-type Czochralski silicon, Journal Applied Physics, 105 (2009) 093704.
[33] D. Macdonald, A. Liu, F. Rougieux, A. Cuevas, B. Lim, J. Schmidt, M. Di Sabatino, L. Geerligs, Boron-oxygen defects in compensated p-type Czochralski silicon, in: Proceedings of 24th European Photovoltaic Solar Energy Conference, Hamburg (Germany), 2009, pp. 877-882.

[34] T. Schutz-Kuchly, J. Veirman, S. Dubois, D.R. Heslinga, Light-Induced-Degradation effects in boron-phosphorus compensated n-type Czochralsky silicon, Applied Physics Letters, 96 (2010) 093505.
[35] K. Tang, E. Øvrelid, G. Tranell, M. Tangstad, A thermochemical database for the solar cell silicon materials, Materials Transactions, 50 (2009) 1978-1984.
[36] R. Kvande, Incorporation of Impurities during Directional Solidification of Multicrystalline Silicon for Solar Cells, in: Doctoral Thesis, 2008:71, NTNU, Trondheim (Norway), 2008.
[37] H. Matsuo, R.B. Ganesh, S. Nakano, L. Liu, Y. Kangawa, K. Arafune, Y. Ohshita, M. Yamaguchi, K. Kakimoto, Thermodynamical analysis of oxygen incorporation from a quartz crucible during solidification of multicrystalline silicon for solar cell, Journal Crystal Growth, 310 (2008) 4666-4671.
[38] C. Hassler, H.U. Hofs, W. Koch, G. Stollwerck, A. Muller, D. Karg, G. Pensl, Formation and annihilation of oxygen donors in multicrystalline silicon for solar cells, Materials Science and Engineering B, 71 (2000) 39-46.
[39] VV.AA., Properties of Crystalline Silicon, INSPEC The Institution of Electrical Engineers, London (United Kingdom), 1999.
[40] H. Nordmark, Microstructure studies of silicon for solar cells, in: Doctoral Thesis, 2009:16, NTNU, Trondheim (Norway), 2009.
[41] H.J. Möller, C. Funke, A. Lawerenz, S. Riedel, M. Werner, Oxygen and lattice distorsions in multicrystalline silicon, Solar Energy Materials & Solar Cells, 72 (2002) 403-416.
[42] H.J. Möller, L. Long, M. Werner, D. Yang, Oxygen and carbon precipitation in multicrystalline solar silicon, Physica Status Solidi, 171 (1999) 175-189.
[43] S. Pizzini, Bulk solar grade silicon: how chemistry and physics play to get a benevolent microstructural material, Applied Physics A - Materials Science and Processing, 96 (2009) 171-188.
[44] K. Jurkschat, S. Senkader, R.P. Wilshaw, D. Gambaro, R.J. Falster, Onset of slip in silicon containing oxide precipitates, Journal Applied Physics, 90 (2001) 3219-3225.
[45] M. Di Sabatino, S. Binetti, J. Libal, M. Acciarri, H. Nordmark, E. Øvrelid, Oxygen distribution on a multicrystalline silicon ingot grown from upgraded metallurgical silicon, Solar Energy Materials & Solar Cells, 95 (2011) 529-533.
[46] Oxygen in silicon, in: Semiconductors and Semimetals, vol. 42, Academic Press, 1994.
[47] J. Veirman, S. Dubois, N. Enjalbert, M. Lemiti, A fast and easily implemented method for interstitial oxygen concentration mapping through the activation of thermal donors in silicon, Energy Procedia, 8 (2011) 41-46.
[48] H. Sun, C. Liu, Q. Hao, L. Wang, Effect of oxygen precipitates in solar grade silicon on minority carrier lifetime and efficiency of solar cells, Rare Metals, 25 (2006) 141-145.
[49] J. Friedl, The role of oxygen in multicrystalline silicon, in: Master Thesis at NTNU, Trondheim (Norway), 2009.
[50] A.R. Gallala, Impact of a two-step heat treatment upon PV multicrystalline silicon, in: Master Thesis at NTNU, Trondheim (Norway), 2010.
[51] M. Sanati, S.K. Estreicher, Boron-oxygen complexes in Si, Physica B, 376-377 (2006) 133-136.
[52] K. Bothe, R. Sinton, J. Schmidt, Fundamental Boron-Oxygen-related carrier lifetime limit in mono- and multi-crystalline silicon, Progress in Photovoltaics: Research and Applications, 13 (2005) 287-296.
[53] J. Schmidt, K. Bothe, Structure and transformation of the metastable boron- and oxygen-related defect center in crystalline silicon, Physical Review B, 69 (2004) 024107.

[54] S. Rein, S.W. Glunz, Electronic properties of the metastable defect in boron-doped Czochralski silicon: Unambiguous determination by advanced lifetime spectroscopy, Applied Physics Letters, 82 (2003) 1054-1056.
[55] K. Bothe, J. Schmidt, Fast-forming boron-oxygen-related recombination center in crystalline silicon, Applied Physics Letters, 87 (2005) 262108.
[56] B. Lim, K. Bothe, J. Schmidt, Impact of oxygen on the permanent deactivation of boron-oxygen-related recombination centers in crystalline silicon, Journal Applied Physics, 107 (2010) 123707.
[57] A. Herguth, G. Schubert, M. Kaes, G. Hahn, Investigations on the long term behavior of the metastable boron-oxygen complex in crystalline silicon, Progress in Photovoltaics: Research and Applications, 16 (2008) 135-140.
[58] B. Lim, A. Liu, D. Macdonald, K. Bothe, J. Schmidt, Impact of dopant compensation on the deactivation of boron-oxygen recombination centers in crystalline silicon, Applied Physics Letters, 95 (2009) 232109.
[59] B. Lim, F. Rougieux, D. Macdonald, K. Bothe, J. Schmidt, Generation and annihilation of boron-oxygen-related recombination centers in compensated p- and n-type silicon, Journal Applied Physics, 108 (2010) 103722.
[60] V.V. Voronkov, R. Falster, A.V. Batunina, D. Macdonald, K. Bothe, J. Schmidt, Lifetime degradation mechanism in boron-doped Czochralski silicon, Energy Procedia, 3 (2011) 46-50.
[61] R. Søndenå, A. Holt, A.-K. Søiland, Light induced degradation in monocrystalline silicon wafers made from the metallurgical route, in: Proceedings of 25th European Photovoltaic Solar Energy Conference, Valencia (Spain), 2010, pp. 1586-1590.
[62] T. Buonassisi, A.A. Istratov, M. Heuer, M.D. Pickett, E.R. Weber, Distinguishing the impacts of individual metal species on multicrystalline silicon performance in a multiple-metal environment, in: Proceedings of 20th European Photovoltaic Solar Energy Conference, Barcelona (Spain), 2005.
[63] J. Schmidt, Effect of dissociation of iron-boron pairs in crystalline silicon on solar cells, Progress in Photovoltaics: Research and Applications, 13 (2005) 325-331.
[64] D. Macdonald, A. Cuevas, M. Di Sabatino, L. Geerligs, Carrier lifetime studies of strongly compensated p-type Czochralski silicon, in: Proceedings of 23rd European Photovoltaic Solar Energy Conference, Valencia (Spain), 2008, pp. 951-957.
[65] G. Coletti, R. Kvande, V. Mihailetchi, L.J. Geerligs, L. Arnberg, E. Øvrelid, Effect of iron in silicon feedstock on p- nd n-type multicrystalline silicon solar cells, Journal Applied Physics, 104 (2008) 104913.
[66] K. Peter, R. Kopecek, M. Wilson, J. Lagowski, E. Enebakk, A.-K. Søiland, S. Grandum, Multicrystalline solar grade silicon solar cells, in: 35th IEEE Phovotoltaic Specialist Conference, Honolulu, USA, 2010.
[67] Y. Boulfrad, E.J. Øvrelid, L. Arnberg, M. Syre, R. Søndenå, Enhancement of the performance of as-grown mc-Si wafers from the deteriorated area of ingots by internal gettering, in: 5th Crystalline Silicon Solar Cells Workshop Boston (USA), 2011.
[68] G. Coletti, P. Bronsveld, G. Hahn, W. Warta, D. Macdonald, B. Ceccaroli, K. Wambach, N. Le Quang, J. Fernandez, Impact of metal contamination in silicon solar cells, Advanced Functional Materials, 21 (2011) 879-890.
[69] S. Martinuzzi, S. Dubois, N. Enjalbert, Minority carrier lifetime and diffusion length in voluntarily chromium contaminated n-type mc-silicon wafers, in: Proceedings of 23rd European Photovoltaic Solar Eenrgy Conference, Valencia (Spain), 2008, pp. 1461-1464.
[70] S. Dubois, N. Enjalbert, F. Servant, F. Garandet, R. Monna, J. Kraiem, Beneficial effects of dopant compensation on carrier lifetime in upgraded metallurgical silicon, in: Proceedings

of 23rd European Photovoltaic Solar Energy Conference, Valencia (Spain), 2008, pp. 1445-1448.
[71] A. Pavel, M. Rezvan Khan, N.E. Islam, On the possibility of improving silicon solar cell efficiency through impurity photovoltaic effect and compensation, Solid-State Electronics, 54 (2010) 1278-1283.
[72] M. Hystad, The distribution and impact of chromium impurities in compensated SoG-silicon, in: Master Thesis at NTNU, Trondheim (Norway), 2009.
[73] D. Saynova, G. Coletti, M. Di Sabatino, L.J. Geerligs, Efficiency potential of solar cells based on compensated multicrystalline silicon materials, in: Proceedings of 25th European Photovoltaic Solar Energy Conference, Valencia (Spain), 2010, pp. 1934-1938.
[74] A.-K. Søiland, Silicon for solar cells, in: Doctoral Thesis at NTNU, 2004:140, Trondheim (Norway), 2004.
[75] L. Raabe, O. Pätzold, I. Kupka, J. Ehrig, S. Würzner, M. Stelter, The effect of graphite components and crucible coating on the behaviour of carbon and oxygen in multicrystalline silicon, Journal Crystal Growth, 318 (2011) 234-238.
[76] C. Londos, M. Potsidi, V. Emtsev, Effect of carbon on oxygen precipitation in Czochraslki silicon, Physica Status Solidi C, 6 (2005) 1963-1967.
[77] A.-K. Søiland, E. Øvrelid, T.A. Engh, O. Løhne, J.K. Tuset, Ø. Gjerstad, SiC and Si_3N_4 inclusions in multicrystalline silicon ingots, Materials Science in Semiconductor Processing, 7 (2004) 39-43.
[78] L.J. Geerligs, P. Manshanden, G.P. Wyers, E.J. Øvrelid, O.S. Raanes, A.N. Wærnes, B. Wiersma, Specification of solar grade silicon: how common impurities affect the cell efficiency of mc-Si solar cells, in: Proceedings of 20th European Solar Energy Conference, 2005, pp. 619-622.
[79] L. Geerligs, D. Macdonald, Base doping and recombination activity of impurities in crystalline silicon solar cells, Progress in Photovoltaics: Research and Applications, 12 (2004) 309-316.
[80] A. Cuevas, The paradox of compensated silicon, in: Proceedings of Conference on Optoelectronics and Microelectronic Materials and Devices (COMMAD), Sidney (Australia), 2008, pp. 238-241.
[81] J. Veirman, S. Dubois, N. Enjalbert, J.P. Garandet, M. Lemiti, Electronic properties of highly-doped and compensated solar-grade silicon wafers and solar cells, Journal Applied Physics, 109 (2011) 103711.
[82] D. Macdonald, A. Cuevas, Recombination in compensated crystalline silicon for solar cells, Journal Applied Physics, 109 (2011) 043704.
[83] G. Stokkan, Characterisation of multicrystalline silicon solar cells. Development of characterisation method for the combined effect of dislocations and grain boundaries on the minority carrier lifetime, in: Doctoral Thesis at NTNU, 2004:58, Trondheim
[84] I. Périchaud, Gettering of impurities in solar silicon, Solar Energy Materials & Solar Cells, 72 (2002) 315-326.
[85] K. Peter, R. Kopecek, A.-K. Søiland, E. Enebakk, Future potential for SoG-Si feedstock from the metallurgical process route, in: Proceedings of 23rd European Phovotoltaic Solar Energy Conference, Valencia (Spain), 2008, pp. 947-950.
[86] D. Kohler, B. Raabe, S. Braun, S. Seren, G. Hahn, Upgraded metallurgical silicon solar cells: A detailed material analysis, in: Proceedings of 24th European Phovotoltaic Solar Energy Conference, Hamburg (Germany), 2009, pp. 1758-1761.
[87] B. Herzog, G. Hahn, Studies of compensation behaviour in mc-silicon, in: Arriving at well-founded SoG silicon feestock specifications Workshop, Amsterdam (Netherlands), 2008.
[88] http://en.wikipedia.org/wiki/Electron_mobility, last accessed: September 2011.

[89] M. Green, Review of semiconductor properties, in: Solar cells. Operating principles, technology and system application, The University of New South Wales, Kensigton (Australia), 1998.
[90] W.R. Runyan, T.J. Shaffner, Mobility, Conductivity Type, and Hall Effect, in: Semiconductor measurements and instrumentation - 2nd ed., McGraw-Hill, New York, 1997, pp. 141-158.
[91] B. Lim, M. Wolf, J. Schmidt, Carrier mobilities in multicrystalline silicon wafers made from UMG-Si, Physica Status Solidi C, 3 (2011) 835-838.
[92] J. Veirman, S. Dubois, N. Enjalbert, J.P. Garandet, D.R. Heslinga, M. Lemiti, Hall mobility reduction in single-crystalline silicon gradually compensated by thermal donors activation, Solid-State Electronics, 54 (2010) 671-674.
[93] F. Schindler, J. Geilker, W. Kwapil, J. Giesecke, M.C. Schubert, W. Warta, Conductivity mobility and Hall mobility in compensated multicrystalline silicon, in: Proceedings of 25th European Solar Energy Conference, Valencia (Spain), 2010, pp. 2364-2368.
[94] F.E. Rougieux, D. Macdonald, A. Cuevas, S. Ruffell, J. Schmidt, B. Lim, A.P. Knights, Electron and hole mobility reduction and Hall factor in phosphorus-compensated p-type silicon, Journal Applied Physics, 108 (2010) 013706.
[95] ASTM F76-86 - Standard test methods for measuring resistivity and Hall coefficient and determining Hall mobility in single-crystal semiconductors.
[96] J.F. Lin, S.S. Li, L.C. Linares, K.W. Teng, Theoretical analysis of Hall factor and Hall mobility in p-type silicon, Solid State Electronics, 24 (1981) 827-833.
[97] J. Brody, A. Rohatgi, V. Yelundur, Bulk resistivity optimization for low-bulk-lifetime silicon solar cells, Progress in Photovoltaics: Research and Applications, 9 (2001) 273-285.
[98] M.C. Flemings, Solidification processing, in, McGraw-Hill, New York, 1974.
[99] S. Fishler, Correlation between maximum solubility limit and distribution coefficient of impurities in Ge and Si, New Jersey, USA, 1962.
[100] ASTM F723-99 - Standard Practice for Conversion Between Resistivity and Dopant Density for Boron-doped, Phosphorus-doped and Arsenic-Doped Silicon, 1999.
[101] E. Good, R. Kopecek, J. Arumughan, Characterizing device efficiency potential from industrial multi-crystalline cell structures composed of solar grade silicon, in: Proceedings of 23rd European Photovoltaic Solar Energy Conference, Valencia (Spain), 2008, pp. 1218-1224.
[102] G. Coletti, Sensitivity of crystalline silicon solar cells to metal impurities, in: 5th Crystalline Silicon Solar Cells, Boston (USA), 2011.
[103] T. Buonassisi, A.A. Istratov, M.D. Pickett, M. Heuer, J.P. Kalejs, G. Hahn, M.A. Marcus, B. Lai, Z. Cai, S.M. Heald, T.F. Ciszek, R.F. Clark, D.W. Cunningham, A.M. Gabor, R. Jonczyk, S. Narayanan, E. Sauau, E. Weber, Chemical natures and distributions of metal impurities in multicrystalline silicon materials, Progress in Photovoltaics: Research and Applications, 14 (2006) 513-531.
[104] W. Kwapil, M. Wagner, M.C. Schubert, W. Warta, High net doping concentration responsible for critical diode breakdown behavior in upgraded metallurgical multicrystalline silicon solar cells, Journal Applied Physics, 108 (2010) 023708.
[105] A. Kassis, M. Saad, Analysis of a multi-crystalline silicon solar cell at low illumination levels using a modified two-diode model, Solar Energy Materials & Solar Cells, 94 (2010) 2108-2112.
[106] Ø. Mjøs, Directional solidification of silicon for solar cells, in: Doctoral Thesis at NTNU, 2006:109, Trondheim (Norway), 2006.
[107] http://en.wikipedia.org/wiki/Four_point_probe_method, last accessed: August 2011

[108] J. Hinrichs, M. Hamester, L. Rottmann, Analysis of solar cell silicon using Glow Discharge Mass Spectrometry, in: Application note: 30164, Thermo Fisher Scientific Inc., Bremen (Germany), 2008.
[109] M. Di Sabatino, A.L. Dons, J. Hinrichs, L. Arnberg, Determination of relative sensitivity factors for trace element analysis of solar cell silicon by fast-flow glow discharge mass spectrometer, Spectrochimica Acta Part B: Atomic Spectroscopy, 66 (2011) 144-148.
[110] Thermo Scientific Element GD - Glow Discharge Mass Spectrometer Manual, in: Thermo Fisher Scientific (Bremen) GmbH, 2009.
[111] http://www.thermoscientific.com/ecomm/servlet/productsdetail_11152_L11308_82243_11961710_-1, last accessed: August 2011.
[112] Introduction to Fourier transform infrared spectrometry, Thermo Nicolet Corporation, 2001.
[113] SEMI, MF1188 - Test method for interstitial atomic oxygen content of silicon by infrared absorption with short baseline.
[114] SEMI, MF1391 - Test method for substitutional atomic carbon content of silicon by infrared absorption.
[115] http://en.wikipedia.org/wiki/Carrier_lifetime, last accesses: August 2011.
[116] M. Green, Generation, recombination, and the basic equations of device physics, in: Solar cells. Operating principles, technology and system application, The University of New South Wales, Kensigton (Australia), 1998.
[117] R. Sinton, A. Cuevas, Contactless determination of current-voltage charateristics and minority-carrier lifetimes in semicounductors from quasi-steady-state photoconductance data, Applied Physics Letters, 69 (1996) 2510-2512.
[118] P. Basore, D. Clugston, PC1D version 4 for Windows: from analysis to desing, in: Conference record of 25th IEEE Photovoltaic Specialists Conference, Washington D.C., USA, 1996, pp. 377-381.
[119] L.J. van der Pauw, A method of measuring the resistivity and Hall coefficient on lamellae of arbitrary shape, Philips Technical Review, 20 (1958) 220-224.

Articles

> œf` ib I

Investigation of bulk and solar cell properties of ingots cast from compensated solar grade silicon

(Progress in Photovoltaics: Research and Applications 19 (2011) 45-53)

Is not included due to copyright

> œf ` ib II

Relationship between net doping density and resistivity compensated mc-Si ingots

(Physica Status Solidi C 8 (2011) 713-716)

Is not included due to copyright

> ocf` ib HHF

Temperature-dependent Hall-effect measurements of p-type multicrystalline compensated solar grade silicon

(Under review in Progress in Photovoltaics: Research and Applications, December 2011)

Is not included due to copyright

Bulk properties of multicrystalline silicon ingots for solar cells cast in silicon nitride crucibles

(To be submitted for publication in Journal Crystal Growth, January 2012)

> œf ib IV

Is not included due to copyright

Distribution and impact of chromium in compensated solar grade silicon

(Under review for publication in Solar Energy Materials & Solar Cells, November 2011)

Is not included due to copyright